Fatty acid synthesis in satellite glial cell promotes regenerative growth in sensory neurons

Oshri Avraham[1], Pan-Yue Deng[2], Sara Jones[1], Rejji Kuruvilla[3], Clay F. Semenkovich[4,2], Vitaly A. Klyachko[2] and Valeria Cavalli[1,5,6,*]

[1] Department of Neuroscience, Washington University School of Medicine, St Louis 63110, Missouri, USA

[2] Department of Cell Biology and Physiology, Washington University School of Medicine, St Louis 63110, Missouri, USA

[3] Department of Biology, Johns Hopkins University, Baltimore 21218, Maryland, USA

[4] Division of Endocrinology, Metabolism & Lipid Research, Washington University School of Medicine, St Louis 63110, Missouri, USA

[5] Center of Regenerative Medicine, Washington University School of Medicine, St. Louis, MO 63110, USA

[6] Hope Center for Neurological Disorders, Washington University School of Medicine, St. Louis, MO 63110, USA

Lead Contact:
Further information and requests for resources and reagents should be directed to and will be fulfilled by the Lead Contact Valeria Cavalli, cavalli@wustl.edu

***Correspondence to**: Valeria Cavalli, Department of Neuroscience, Washington University School of Medicine, Campus Box 8108, 660 S. Euclid Ave, St. Louis, MO 63110-1093 Phone: 314 362 3540, Fax: 314 362 3446, E-mail: cavalli@wustl.edu

SUMMARY

Peripheral sensory neurons switch to a regenerative state after nerve injury to enable axon regeneration and functional recovery. Whether satellite glial cells (SGC), which completely surround the neuronal soma, contribute to the regenerative responses remains unexplored. Here we defined the transcriptional profile of SGC and identified Fabp7/BLBP as a novel marker of SGC. We report that nerve injury changes gene expression in SGC, which is mostly related to lipid metabolism, specifically fatty acid synthesis and PPARα signaling. Conditional deletion of Fatty acid synthase (Fasn), the committed enzyme in *de novo* fatty acid synthesis in SGC impairs axon regeneration. Treatment with the PPARα agonist fenofibrate rescues axon regeneration in mice lacking Fasn in SGC. This results indicates that PPARα functions downstream of fatty acid synthesis in SGC to promote axon regeneration. These results identify fatty acid synthesis in SGC as a fundamental novel mechanism mediating axon regeneration in adult peripheral nerves.

INTRODUCTION

Unlike neurons in the central nervous system, peripheral sensory neurons with cell soma in dorsal root ganglia (DRG) switch to a regenerative state after nerve injury to enable axon regeneration and functional recovery. Decades of research have focused on the signaling pathways elicited by injury in sensory neurons (He and Jin, 2016; Mahar and Cavalli, 2018) and in Schwann cells that insulate axons (Chen et al., 2007b; Jessen and Mirsky, 2016) as central mechanisms regulating nerve repair. However, virtually nothing is known about the contribution of the glial cells that envelop the neuronal soma, known as satellite glial cells (SGC), to the nerve repair process.

In adult animals, multiple SGC form an envelope that completely enwraps each sensory neuron (Hanani, 2005; Pannese, 1981, 2010). The number of SGC surrounding sensory neurons increases with increasing soma size in mammals (Ledda et al., 2004; Pannese, 1964). The neuron and its surrounding SGC thus form a distinct morphological and functional unit. Structural neuron-glia units ,similar to these, do not exist in the central nervous system. SGC have been identified mostly based on their morphology and location. Several SGC markers have been characterized, including the inwardly rectifying potassium channel (Kir4.1) (Vit et al., 2008), cadherin 19 (CDH19) (George et al., 2018), the calcium activated potassium channel (SK3) (Donegan et al., 2013; Vit et al., 2006) and glutamine synthetase (GS) (Hanani, 2005; Miller et al., 2002). SGC also share several properties with astrocytes, and express glial fibrillary acidic protein (GFAP) (Hanani, 2005; Stephenson and Byers, 1995).

SGC have been studied in the context of pain responses and are known to modulate pain thresholds (Hanani, 2015; Huang et al., 2010; Jasmin et al., 2010; Kim et al., 2016b; Warwick and Hanani, 2013). It is known that SGC are altered structurally and functionally under pathological conditions, such as inflammation, chemotherapy-induced neuropathic pain and nerve injuries (Cherkas et al., 2004; Hanani, 2005; Hanani et al., 2002; Warwick and Hanani, 2013). Nerve lesions also induce an increase in GFAP expression (Christie et al., 2015; Fenzi et al., 2001;

Warwick and Hanani, 2013; Xie et al., 2009; Xu et al., 2008; Zhang et al., 2009). Increase in p75 and pERK expression has also been observed in SGC after nerve lesions (Obata et al., 2004; Zhou et al., 1996). An increase in SGC ongoing cell division following nerve injury has also been suggested (Christie et al., 2015; Krishnan et al., 2018). These studies show that communication between neuron and SGC is critical for neuronal excitability and nociception and that SGC can sense and respond to a distant nerve injury (Huang et al., 2013; Kung et al., 2013), but whether SGC play a role in regenerative responses has not yet been established.

Using single cell RNA-seq, we reveal that nerve injury alters the gene expression profile in SGC, which is mostly related to lipid metabolism, including fatty acid synthesis. Conditional deletion of Fatty acid synthase (Fasn), the committed enzyme in *de novo* fatty acid synthesis, specifically in SGC, impairs axon regeneration in peripheral nerves. Treatment with fenofibrate, a PPARα agonist, rescues the impaired axon regeneration observed in mice lacking Fasn in SGC, suggesting that PPARα functions downstream of fatty acid synthesis in SGC to promote axon regeneration. These results unravel lipid synthesis in SGC as a fundamental novel mechanism mediating axon regeneration in adult peripheral nerves.

RESULTS

Single-cell transcriptional profiling identified multiple cell types in naïve and injured DRG

To define the biology of SGC and to understand the role of SGC in nerve injury responses, we performed single cell RNA-seq (scRNA-seq) of mouse L4,L5 DRG in naïve and injured conditions (3 days post sciatic nerve crush injury), using the Chromium Single Cell Gene Expression Solution (10x Genomics) (Figure 1A). Graph-based clustering, using Partek flow analysis package, identified 13 distinct cell clusters in the control and injury samples (Figure 1B). Unique cell clusters were not altered by nerve injury (Figure 1C). The total of sequenced cells was 6,541 in 2 biological replicates, with an average of 45,000 reads per cell, 1,500 genes per

cell and a total of 17,879 genes detected. To identify cluster-specific genes, we calculated the expression difference of each gene between that cluster and the average in the rest of the clusters (ANOVA fold change threshold >1.5), illustrated by a heatmap of the top 5 differentially expressed genes per cluster relative to all other clusters (Figure 1D and Table 1). Examination of the cluster-specific marker genes revealed major cellular subtypes including neurons (Isl1), SGC (KCNJ10/Kir4), Schwann cells (Periaxin, MPZ), endothelial cells (Pecam1/CD31), macrophages (Alf1/Iba-1, CD68), mesenchymal (CD34) connective tissue (Col1A1), T-cells (CD3G) and Vasculature associated smooth muscle cells (DES). Overlaid cells in t-SNE plots with well characterized marker genes show the relative levels of expression as a color gradient (Figure 1E,F and S1A). We anticipated obtaining a larger representation of neurons in our dataset, but their large cell diameter (up to 50 micron for proprioceptors), is likely limiting them from passing through the microfluidic pipes in the Chromium 10X device.

SGC are molecularly distinct from Schwann cells in DRG

The scRNAseq results indicate that SGC represent the largest glial subtype (35%) in the DRG and are molecularly distinct from Schwann cells. The SGC cluster identity was confirmed by the expression of known SGC markers such Kir4.1 (Vit et al., 2008) and CDH19 (George et al., 2018) (Figure 1E). While Schwann cells and SGC share the expression of known Schwann cell markers, such as MPZ, MBP and PLP1 (Figure 1F and S1B), our analysis also revealed Schwann cell specific marker genes such as Myelin Associated Glycoprotein (MAG), Periaxin (PRX) and Non-Compact Myelin Associated Protein (NCMAP) genes that are not expressed in SGC (Figure 1G and S1B). We next compared the top expressed genes in SGC (605 genes) and Schwann cells (572 genes), which revealed that SGC share only 2% of genes with Schwann cells in the DRG (Figure S1C and Table 2). SGC also share several properties with astrocytes, including expression of Kir4.1 and glial fibrillary acidic protein (GFAP) (Hanani, 2005; Stephenson and Byers, 1995; Vit et al., 2008). We thus examined the transcriptional similarity between

astrocytes and SGC by comparing the top expressed genes in each cell type, using our scRNAseq data for SGC and a previously published transcriptional analysis of astrocytes (500 genes) (Zhang et al., 2014). We found that SGC share about 10% of genes with astrocytes, among them Fabp7, Gfap, Ppara and Aldoc (Figure S1D, Table 2). Our single cell RNAseq analysis using freshly dissociated tissue thus unravel a unique transcriptional profile of SGC in DRG and reveals that Schwann cells and SGC are transcriptionally distinct in the DRG.

Fatty acid binding protein7 is a specific marker for adult mouse SGC.

The scRNAseq data revealed that one of the top differentially expressed genes in the SGC cluster is Fatty Acid Binding Protein 7 (Fabp7, also known as BLBP and BFABP) (Table 1, Figure S1C). Fabp7 is a nervous system specific member of the hydrophobic ligand binding protein family involved in uptake and transport of fatty acid (Furuhashi and Hotamisligil, 2008). Fabp7 is involved in signal transduction and gene transcription in the developing mammalian CNS (Feng et al., 1994), but its precise function remains quite elusive. In the peripheral nervous system, Fabp7 is expressed during embryonic development and distinguishes glia from neural crest cells and neurons during the early stages of development (Britsch et al., 2001; Kastriti and Adameyko, 2017; Weider et al., 2015). These observations prompted us to test if Fabp7 can be used as a novel marker of SGC in adult mouse DRG. We found that Fabp7 labels SGC surrounding sensory neuron soma (Figure 2A). The specificity of the Fabp7 antibody was verified using DRG and sciatic nerve from the Fabp7KO mouse (Owada et al., 2006) (Figure S2A-C), in which Fabp7 signal surrounding neurons is lost, but SGC are present and stained with glutamine synthetase (GS) (Hanani, 2005; Miller et al., 2002). Importantly, Fabp7 does not label Schwann cells surrounding axons in the DRG (Figure 2A, asterisks), or in the sciatic nerve (Figure S2C) consistent with previous reports (Kurtz et al., 1994; Miller et al., 2003) and our single cell analysis (Figure 2B).

We next tested if the BLBPcre-ER mouse line (Maruoka et al., 2011) can be used to label and manipulate SGC specifically. We crossed BLBPCre-ER to the Rosa26-fs-TRAP and observed that following 10 days tamoxifen treatment, BLBPcre-ER mice drove expression of the GFP reporter in SGC (Figure 2C, upper panel). To further ensure that the BLBPcre-ER is specifically expressed in SGC in the DRG and does not drive expression in Schwann cells in the nerve, we crossed BLBPcre-ER to the Sun1-sfGFP-myc (INTACT mice: R26-CAG-LSL-Sun1-sfGFP-myc) (Mo et al., 2015), which allows GFP expression in the nuclear membrane. We found GFP positive nuclei around the neurons in DRG sections (Figure 2C, lower panel) and no nuclear GFP expression axons in naïve sciatic nerves (Figure 2D). Since a role for Fabp7 in regulating Schwann cell-axon interactions has been proposed (Miller et al., 2003), with Fabp7 expressed 2 to 3 weeks after nerve injury when Schwann cell process formation is exuberant, we also examined nuclear GFP expression in injured nerves. We found that 3 days post injury, 4% and 7% of the nuclei expressed the GFP reporter proximal and distal to the injury site, respectively (Figure 2D,E). This is consistent with a prior report showing that BLBP is not present 4 to 7 days post injury, but is expressed in some cells starting 14 days post injury (Miller et al., 2003). Since typically, 50% of nuclei express c-jun, a marker for Schwann cells response to injury, two days after injury in the nerve (Blom et al., 2014), the GFP positive nuclei we observed, may represent a very small subset of Schwann cells responding to injury. To further confirm the specificity of the BLBPCreER reporter following nerve injury, we re-analyzed a single cell data set from injured nerve (9 days post injury) (Carr et al., 2019). We found that less than 5% of cells in the Schwann cell cluster expressed Fabp7 (Figure S2D). A comparative analysis of the transcriptome of injured nerve (3 days post injury) also demonstrated very low counts of Fabp7 in proximal and distal nerve segments (Shin et al., 2018). Together, these experiments reveal that Fabp7 represents a novel marker of SGC and that the BLBPcre-ER mouse line can be used to label and manipulate SGC, with only minimal impact on Schwann cells at early time points after nerve injury.

SGC upregulate lipid metabolism in response to nerve injury

To define the transcriptional response of SGC to nerve injury, cells in the SGC cluster were pooled and control and injury conditions were compared to identify differentially expressed genes. 1,255 genes were differentially upregulated in SGC after injury (FDR>0.05, Log2Fold change>2) (Table 3) and analyzed for enriched biological pathways using KEGG 2016 (Kyoto Encyclopedia of Genes and Genomes). This analysis revealed enrichment in lipid metabolic pathways, including fatty acid biosynthesis (Figure 3A). Pathway analysis of other major cells types in the DRG confirmed fatty acid metabolism as a unique pathway enriched in SGC in response to nerve injury (Figure S3A-F). Although both SGC and macrophages were suggested to undergo cell cycle after nerve injury (Krishnan et al., 2018), our pathway analysis indicate that the cell cycle term is enriched in macrophages, but not SGC (Figure 3 and S3A).

One of the genes enriched in SGC is fatty acid synthase (Fasn), the committed enzyme in *de novo* fatty acid synthesis (Dean and Lodhi, 2018) (Figure 3B and Table 2). Immunostaining of DRG sections confirmed Fasn expression in SGC surrounding sensory neuron soma (Figure 3C, upper panel). These observations prompted us to investigate the role of Fasn in SGC. We generated an SGC specific *Fasn* KO mouse (FasncKO) by crossing BLBPcre-ER (Maruoka et al., 2011) mice to mice carrying floxed *Fasn* alleles (Chakravarthy et al., 2005). 8 week old BLBPcre-ER;Fasn$^{f/f}$ (FasncKO) and BLBPcre-ER^{-};Fasn$^{f/+}$ mice (control) were fed with tamoxifen for 10 days to conditionally delete *Fasn* in SGC. This design allows us to ensure that both control and FasncKO groups are treated with tamoxifen and thus differences between groups do not result from the tamoxifen treatment itself. Expression of Fasn in SGC visualized by immunofluorescence was significantly reduced in the FasncKO DRG compared to control littermates (Figure 3C, bottom panel). Western blot analysis of Fasn in DRG also confirmed reduction of Fasn expression in the FasncKO compared to control littermates (Figure 3E). Fasn has been shown to be expressed in Schwann cells (Montani et al., 2018), and immunostaining for Fasn in the sciatic nerve confirms

these results (Figure 3D,E). However, Fasn expression was not affected in the nerve of FasncKO mice (Figure 3D,E and F) confirming the specificity of the BLBPCre-ER line for SGC.

Deletion of Fasn in SGC does not alter SGC morphology or functional properties.

To determine the impact of Fasn deletion on SGC morphology, we performed transmission electron microscopy (TEM), as previously reported (Pannese, 1964, 2010). We observed no abnormalities in the morphology of the SGC surrounding the neuron somas in the FasncKO animals compared to controls (Figure 4A, SGC were pseudo colored). The SGC sheath is smooth and separated from the sheaths enclosing the adjacent nerve cell bodies by a connective tissue space, as described extensively previously (Pannese, 1964, 2010). The SGC coat is also in direct contact with the neuronal membrane, as described (Pannese, 1964, 2010). We next evaluated both Remak bundle structure and myelin sheath thickness in the nerve of the FasncKO mice compared to control animals (Figure 4B-F). Neither the number of axons per Remak bundle nor the myelin thickness and axon diameter was altered in the FasncKO. To confirm that the reduction of Fasn in SGC does not cause neuronal cell death, we immunostained sections of DRG from FasncKO and control mice for the apoptotic marker cleaved caspase 3 before and after injury (Figure S4A). Quantification of Caspase 3 intensity revealed no change in cell death in naïve conditions and three days post injury between FasncKO and control (Figure 4G and S4A). We next examined the expression of Atf3, an established neuronal injury marker (Holland et al., 2019; Mahar and Cavalli, 2018). Atf3 levels in control and FasncKO animals were very low in the absence of injury (Figure 4H), indicating that in naïve condition, Fasn deletion in SGC did not cause a stress response in DRG neurons. Nerve injury increased the mRNA levels of Atf3 in control and FasncKO DRG, but this response was less robust in the FasncKO (Figure 4H), Together, these results indicate that loss of Fasn in SGC does not lead to morphological deficits in the DRG and does not elicits a stress response in neurons.

The robust bidirectional communication between neurons and SGC is critical for neuronal excitability and nociception (Huang et al., 2013) and the excitability of sensory neurons is controlled in part by the surrounding SGC (Chen et al., 2015; Kim et al., 2016b; Suadicani et al., 2010; Zhang et al., 2007; Zhang et al., 2005). To examine whether Fasn deletion in SGC affected functional properties of DRG neurons, we compared intrinsic excitability and firing properties of DRG neurons from FasncKO and control mice. Whole-cell recordings were performed in acutely dissociated co-cultures of DRG neurons and glia. Medium diameter neurons that were associated with at least one glial cell were targeted for recordings (Figure S4B). A subset of recorded cells was filled with biocytin via the patch pipette for *post hoc* verification of neuronal identity. The vast majority of filled cells were identified as IB4-positive nociceptors (Figure S4C). We observed that all major features of intrinsic neuronal excitability were unaffected in DRG neurons from FasncKO mice compared to controls, including the resting membrane potential (Figure 4I), membrane capacitance (Figure 4J), and input resistance (Figure 4K). We further examined the spiking properties of DRG neurons and found no detectable changes in action potential threshold (Figure 4M), which represents the principle determinant of neuronal excitability, or the neuronal firing frequency (Figure 4L,N) in FasncKO mice compared to controls. Therefore, Fasn deletion in SGC does not affect functional properties of DRG neurons.

Deletion of Fasn in SGC impairs axon regeneration.

We observed that Atf3 expression after injury was reduced in FasncKO compared to control (Figure 4H), suggesting that absence of Fasn in SGC may impact the neuronal response to injury. To test the consequence of Fasn deletion in SGC on axon regeneration, we used our established *in vivo a*nd ex-vivo regeneration assays (Cho and Cavalli, 2012; Cho et al., 2015; Cho et al., 2013). Two weeks after tamoxifen treatment, we performed a sciatic nerve crush injury in FasncKO and control mice and measured the extent of axon regeneration past the injury site three days later by labeling nerve sections with SCG10, a marker for regenerating axons (Shin et

al., 2014). Loss of Fasn in SGC impaired axon regeneration, demonstrated by reduced axonal length and lower regeneration capacity (Figure 5A-C). We also tested if loss of Fasn has an effect on the conditioning injury paradigm, in which a prior nerve injury increases the growth capacity of neurons (Smith and Skene, 1997). Isolated DRG neurons from naïve and injured FasncKO and control mice were cultured for 20h (Figure 5D). In naïve animals, typically only few neurons extend short neurites, whereas a prior injury leads to more neurons initiating neurite growth and longer neurites (Figure 5D-F). In FasncKO mice, naïve neurons presented similar neurite length to control naïve animals with a similar initiation rate. In contrast, a prior injury in FasncKO mice only partially conditioned the neurons for growth. Neurons in injured FasncKO displayed reduced neurite length compared to injured controls, but similar initiation rates (Figure 5D-F). These results indicate that Fasn in SGC is required for the conditioning effect, and specifically for the elongating phase of axon growth.

Activation of PPARα in SGC contributes to axon regeneration

To understand the mechanism by which Fasn in SGC regulates axon regeneration, we examined the role of peroxisome proliferator-activated receptors (PPARs), which represent a unique set of lipid regulated transcription factors (Varga et al., 2011). Fasn synthesizes palmitic acid, which is the substrate for the synthesis of more complex fatty acids (Dean and Lodhi, 2018). In the liver, Fasn is required for generating the endogenous ligand for PPARα (Chakravarthy et al., 2009), whereas in adipose tissue, Fasn, is required for generating endogenous ligands for PPARγ (Lodhi et al., 2012). Our scRNAseq analysis revealed that PPARα, but not PPARγ, was enriched in the SGC cluster, along with known PPARα target genes PPARGC1α, FADS2 and PEX11A (Rakhshandehroo et al., 2010) (Figure 6A). These PPARα target genes were also upregulated after injury in the SGC cluster (Figure 6B and Table 3). PPARα regulates the expression of genes involved in lipid and carbohydrate metabolism (Varga et al., 2011). This is

consistent with our GO analysis of upregulated genes after injury that indicated an enrichment of the PPAR signaling pathway and lipid metabolism in SGC after injury (Figure 3A and S3). We further confirmed the enrichment of PPARα target genes in SGC vs. neurons using the RNAseq data set from purified nociceptors in naïve condition and 3 days post injury (Carlin et al., 2019) (Figure 6B). These observations indicate that PPARα signaling is enriched in the SGC cluster and suggest that fatty acid synthesis in injured SGC regulate PPAR-dependent transcription.

Whereas biologic PPARα agonists consist of a broad spectrum of ligands (Rakhshandehroo et al., 2010), synthetic PPARα agonists include clofibrate, fenofibrate, bezafibrate, gemfibrozil, Wy14643 and GW7647. To test the effect of these PPARα agonists on axon regeneration, we modified our spot culture assay, in which embryonic DRG are dissociated and cultured in a spot, allowing axons to extend radially from the spot (Cho and Cavalli, 2012; Cho et al., 2013). By not including the mitotic inhibitor 5-deoxyfluoruridine (FDU) to eliminate dividing cells, we observed SGC, labeled with Fabp7 in the cell soma area, where they surround neurons by DIV7 (Figure 6C, S5A,B) but not in the axon region (Figure 6C, S5A,B). The PPARα agonists clofibrate, fenofibrate, Wy14643 and GW7647 were added to the media at 2 concentrations (10μM and 100nM) at DIV6. Axons were cut using a microtome blade at DIV7 and allowed to regenerate for 24h, fixed and stained for SCG10 to visualize axon regeneration (Shin et al., 2014). Regenerative length was measured from the visible blade mark to the end of the regenerating axon tips (Figure 6D,E). Whereas Wy14643 and GW7647 had no effect on axonal regeneration compared to DMSO, clofibrate (100nM) and fenofibrate (100nM, 10μM) increased axon growth after axotomy (Figure 6E). However, clofibrate at a higher concentration (10μM) caused cell death and axonal degeneration. To ensure that the increased regeneration effect was mediated by SGC and was not due to PPAR activation in neurons, we tested fenofibrate, clofibrate and GW7647 in spot cultures treated with FDU, in which no Fabp7 positive cells was detected at DIV7 (Figure S5B). In these conditions, we observed no increase in axon regeneration (Figure 6F

and S5C). These results indicate that activation of PPARα signaling in SGC promote axon growth, although we cannot fully exclude that other cell types present in the spot culture contribute to this effect.

Activation of PPARα with fenofibrate rescues the impaired axon regeneration in FasncKO mice

In the absence of Fasn in SGC, PPARα may lack its endogenous agonist and PPARα signaling following nerve injury may be compromised. To test this hypothesis, we determined if fenofibrate can rescue the axon regeneration defects that we observed in the FasncKO mice. We chose fenofibrate for these *in vivo* experiments because it is FDA-approved to treat dyslipidemia (Rosenson, 2008), is a specific PPARα agonist with minimal activity towards PPARγ and can be delivered easily in the diet (Kim et al., 2016a). Control and FasncKO mice were fed with chow supplemented with fenofibrate, as described (Kim et al., 2016a) for 2 weeks prior to nerve injury. PPARα as well as PPARα target gene expression were upregulated in the DRG of fenofibrate fed mice compared to mice fed with a normal diet (Figure 7A). The impaired axon regeneration in FasncKO mice was rescued by the fenofibrate diet (Figure 7B-D). The fenofibrate diet also rescued the impaired axon growth in the conditioning paradigm (Figure 7E,F), with no change in initiation rate (Figure 7G). These results are consistent with the notion that in response to axon injury, Fasn expression in SGC activates PPARα signaling to promote axon regeneration in adult peripheral nerves.

DISCUSSION

The role of SGC in nerve regeneration has been largely ignored and the biology of SGC is very poorly characterized under normal or pathological conditions. Our unbiased single cell approach characterized the molecular profile of SGC and demonstrated that SGC play a

previously unrecognized role in peripheral nerve regeneration, in part via injury induced activation of PPARα signaling.

SGC have been identified mostly based on their morphology and location. Several SGC markers have been characterized, but no useful markers that can be used to purify SGC and understand their biology at the molecular level have been identify so far. Although a previous study reported that SGC are very similar to Schwann cells (George et al., 2018), this conclusion was drawn from the analysis of cultured and passaged SGC and Schwann cells. Other SGC isolation methods rely on immunoreactivity to SK3 (Jager et al., 2018) or on multiple sucrose gradients and cell plating (George et al., 2018). Our single cell approach provides the advantage of minimal time between dissociation and analysis and is capturing more accurately the actual transcription status of the cells. Using this method, we demonstrate that SGC represent a unique cell population in the DRG, which share some molecular markers with Schwann cells as well as astrocytes. We also characterized a new marker for adult SGC and a mouse line, BLBP-creER (Maruoka et al., 2011), that can be used to manipulate SGC specifically in the DRG. Because Fabp7 is expressed in radial glial cells as well as neuronal progenitors and is critical for neurogenesis in the CNS (Feng et al., 1994; Matsumata et al., 2016; Matsumata et al., 2012), this mouse line needs to be used in an inducible manner in adult mice to avoid targeting other cells during development. It is also important to note that Fabp7 is expressed in astrocytes, where it is important for dendritic growth and neuronal synapse formation (Ebrahimi et al., 2016) as well as for astrocyte proliferation during reactive gliosis (Sharifi et al., 2011), and thus the BLBP-creER line will also target astrocytes in the central nervous system. SGC are believed to share common features with astrocytes, such as expression of Kir4.1 and functional coupling by gap junctions (Christie et al., 2015; Donegan et al., 2013; Hanani, 2005; Huang et al., 2005), with SGC surrounding the same neuron connected by gap junctions. The BLBP-creER mouse line thus represents a new tool to study SGC in the peripheral nervous system.

PPARs are ligand-activated nuclear receptors with the unique ability to bind lipid signaling molecules and transduce the appropriate signals derived from the metabolic environment to control gene expression (Varga et al., 2011). Accordingly, PPARs are key regulators of lipid and carbohydrate metabolism. PPARs can sense components of different lipoproteins and regulate lipid homeostasis based on the need of a specific tissue (Lee et al., 2003). Three different PPAR subtypes are known; PPARα, PPARβ/δ and PPARγ (Lee et al., 2003). All share the same molecular mode of activation, forming a heterodimer with the nuclear receptor RXR, followed by binding to specific DNA-response elements in target genes (PPAREs). PPARγ is important in neurons for axon regeneration (Lezana et al., 2016). However PPARγ is not expressed in SGC according to our scRNAseq data. Rather, our results indicate that PPARα is enriched in SGC and required for efficient nerve regeneration. Fenofibrate is a specific PPARα agonist, making it unlikely that the rescue effects we observed in FasncKO mice are due to activation of PPARγ in neurons. PPARα and PPARα target genes are also highly enriched in SGC, suggesting that fenofibrate act on SGC rather than other resident cells in DRG to enhance axon regeneration. Furthermore, we show that fenofibrate does not improve axon regeneration in neuronal cultures that do not contain SGC. Fenofibrate is used clinically to treat lipid disorders, but has been unexpectedly been shown in clinical trials to have neuroprotective effects in diabetic retinopathy (Bogdanov et al., 2015; Moreno and Ceru, 2015) and in traumatic brain injury (Chen et al., 2007a). Our findings suggest that fenofibrate may be used to activate SGC and enhance axon regeneration in circumstances with poor sensory axon growth, such as after injury to dorsally projecting sensory axons in the spinal cord or peripheral nerve repair. Although fenofibrate treatment did not improve locomotor recovery following spinal contusion injury in mice (Almad et al., 2011), a slight trend for increased tissue sparing was observed. Whether fenofibrate can improve centrally projecting sensory axon growth will need to be rigorously tested.

Biologic PPARα agonists consist of saturated and unsaturated fatty acids, eicosanoids and glucocorticoids (Lee et al., 2003). Fasn synthesizes palmitic acid, which is the substrate for the synthesis of more complex fatty acids (Dean and Lodhi, 2018). Fasn is partially localized in peroxisomes, where ether lipids such as plasmalogens are synthesized (Dean and Lodhi, 2018). In the liver, Fasn is required for generating the endogenous ligand for PPARα (Chakravarthy et al., 2009), whereas in adipose tissue, Fasn is required for generating endogenous ligands for PPARγ (Lodhi et al., 2012). One interpretation of our findings is that in SGC, Fasn is required to generate ligands for PPARα and that following nerve injury, Fasn dependent lipid metabolism and PPARα target genes are upregulated to promote axon regeneration.

How do lipid metabolism and PPARα signaling in SGC contribute to stimulate axon regeneration? Although addressing this question will require further investigation, our data indicate that Fasn expression in SGC is required for the proper expression of at least one regeneration associated gene after injury, Atf3. This finding suggests that SGC contribute to regulate gene expression in neurons. It is also plausible that SGC impact neurons through lipid transfer. Indeed, lipids can be exogenously supplied by lipoproteins secreted from glial cells to stimulate neurite growth. Several studies have suggested a role for ApoE, a PPARα target gene, in lipid delivery for growth and regeneration of axons after nerve injury (Li et al., 2010; Vance et al., 2000; Vance et al., 1994) and ApoE expression is increased in glial cells after nerve injury (LeBlanc and Poduslo, 1990; Snipes et al., 1986). In agreement with these previous reports, our data indicate that ApoE mRNA levels are elevated in SGC after nerve injury and also following fenofibrate treatment (Figure 6B and 7A). In astrocytes, lipid metabolism is critical for synapse development and function *in vivo* (Barres and Smith, 2001; van Deijk et al., 2017). It will therefore be interesting to determine if lipid metabolism in SGC play a direct role in axon regeneration through paracrine effects on neurons.

ACKNOWLEDGMENTS

We would like to thank members of the Cavalli lab for valuable discussions. We would like to thank the following investigators for their generous gifts of mouse lines: Dr. Toshihiko Hosoya for the BLBP-cre ER mice, Dr. Yuji Oawada for the Fabp7KO mice and Dr. Harrison Gabel for the Sunf1GFP mice. We gratefully acknowledge Greg Strout, Ross Kossina and Dr. James Fitzpatrick from the Washington University Center for Cellular Imaging (WUCCI), which is supported in part by Washington University School of Medicine, The Children's Discovery Institute of Washington University, and St. Louis Children's Hospital (CDI-CORE-2015-505 and CDI-CORE-2019-813) and the Foundation for Barnes-Jewish Hospital (3770) for assistance in acquiring and interpreting Transmission Electron Microscopy (TEM) data. We also thank Anushree Seth and Madison Mack in association with InPrint for illustration in Figure1A. This work was funded in part by The McDonnell Center for Cellular and Molecular Neurobiology.

AUTHOR CONTRIBUTIONS

O.A, P.D, R.K, C.S, V.K and VC designed research as well as edited and approved the manuscript; O.A performed sequencing, bioinformatics, *in vitro* and *in vivo* experiments, analyzed the data and wrote the manuscript; P.D performed electrophysiological recordings experiments; S.J. analyzed and quantified in vitro and in vivo regeneration assays and TEM images.

DECLARATION OF INTERESTS

The authors declare no competing interests.

FIGURE LEGENDS

Figure 1: Characterization of cell populations in the DRG

(A) Schematic of the experimental design for scRNAseq

(B) t-SNE plot of 6,541 cells from L4,L5 mouse dissociated DRG, with 13 distinct cell clusters (Graph based clustering). Classifications were assigned based on known marker genes.

(C) t-SNE plot of cells from naïve (blue) and injury (red) conditions.

(D) Heatmap of the top five differentially expressed genes per cluster relative to all other clusters.

(E) t-SNE overlaid for expression of marker genes for SGC,

(F) t-SNE overlaid for expression of marker genes for Schwann cells and SGC

(G) t-SNE overlaid for expression of marker genes for Schwann cell only.

Figure 2: **Fabp7 is a specific marker for SGC**

(A) Representative images of immunofluorescence staining of mouse DRG sections with Fabp7 (green) which labels SGC surrounding neurons marked with Tuj1 (red). No Fabp7 expression in the axon rich area (asterisks) is observed. n=3, Scale bar: 100 μM.

(B) t-SNE overlay of the SGC enriched gene Fabp7

(C) BlbpCreER mice crossed with RosaGFP or Sun1GFP show expression of GFP in the SGC surrounding the neurons marked with Tuj1 (red). RosaGFP n=3, Sun1GFP n=4 Scale bar: 50 μM .

(D) Sciatic nerves from BlbpCreER mice crossed with Sun1GFP. Represented images from naive and injured nerves, proximal and distal to the injury site. n=4 Scale bar: 50 μM.

(E) Quantification of GFP positive nuclei normalized to the total number of dapi positive nuclei. One-way analysis of variance (ANOVA) Sidak's multiple comparisons test. *$p<0.05$ **$p<0.005$; **** $p<0.0001$.

Figure 3: SGC upregulate genes involved in lipid metabolism in response to nerve injury

(A) Pathway analysis (KEGG 2016) of differentially upregulated genes in the SGC cluster. (FDR<.05, Log2Fold change>2)

(B) t-SNE overlay for expression of Fasn gene.

(C) DRG sections from control and FasncKO mice, immunostained for Fasn (green) and the neuronal marker Tuj1 (red) n=3. C, Scale bar: 50 μm

(D) Nerve sections from control and FasncKO mice, immunostained for Fasn (green) and the neuronal marker Tuj1 (red) n=3. C, Scale bar: xx μm.

(E) Western blot analysis of Fasn protein expression in DRG and sciatic nerve from control and FasncKO mice.

(F) Quantification of Fasn expression normalized to Gapdh expression. n=3. One way ANOVA. Dunnett's multiple comparisons test. **p<0.005 ns-non significant.

Figure 4: Fatty Acid synthase deletion in SGC does not alter SGC morphology or functional properties

(A) Representative TEM images of a DRG cell body and its enveloping SGC sheath, pseudo-colored in turquoise, from control and FasncKO mice. Scale bar: 5 μM

(B) Representative TEM images of sciatic nerve cross sections from control and FasncKO mice. Scale bar: 5 μM.

(C) Quantification of average axon diameter in sciatic nerves of FasncKO mice

(D) Average G-ratio in sciatic nerves of FasncKO mice

(E) Linear correlation of G-ratio versus axon diameter in sciatic nerves of FasncKO mice compared with controls. n=3 Unpaired t-test ns-non significant.

(F) Quantification of the number of axons per Remak bundle in FasncKO and control nerves. n=3 Unpaired t-test ns-non significant.

(G) Quantification of cleaved caspase 3 in DRG sections from control and FasncKO mice in naïve and 3 days after sciatic nerve injury. Ratio of Cleaved caspase3 positive vs. dapi was measured. n=4 One way ANOVA ns-non significant.

(H) qPCR analysis of ATF3 expression in DRG from control and FasncKO mice in naïve and 3 days after sciatic nerve injury n=3 One way ANOVA. Sidak's multiple comparisons test **p<0.005 ***p<0.0005 ns-non significant.

(I) Whole-cell recordings were performed in dissociated co-cultures of DRG neurons surrounded by glia from FasncKO and control mice. Quantification of resting membrane potential (RMP) was measured in control -45.3 ± 2.7 mV, n = 16; FasncKO -46.1 ± 1.8 mV, n = 30; p = 0.79;

(J) membrane capacitance (control 18.3 ± 1.8 pF, n = 16; FasncKO 16.5 ± 1.1 pF, n = 30; p = 0.36;

(K) Input resistance (control 456 ± 43 MΩ, n = 16; FasncKO 482 ± 24 MΩ, n = 30; p = 0.56;

(L) Spiking properties of DRG neurons from controls and FasncKO.

(M) Potential threshold (control -9.46 ± 0.94 mV, n = 13; FasncKO -9.91 ± 0.84 mV, n = 28; p = 0.77 and

(N) Neuronal firing rate (control 11.57 ± 2.09 Hz, n = 14; FasncKO 10.62 ± 0.86 Hz, n =29; p = 0.62 was measured. t-test, ns- non significant.

Figure 5: Fatty acid synthase deletion in SGC impairs axon regeneration

(A) Representative longitudinal sections of sciatic nerve from control and FasncKO mice 3 days after sciatic nerve injury, stained for SCG10. Orange lines indicate the crush site, identified

as the maximal SCG10 intensity. Arrowheads indicate longest regenerating axons. Scale bar: 500μM

(B) Length of the longest 10 axons was measured in 10 sections for each nerve. n=8. Unpaired t-test ****$p<0.0001$.

(C) Regeneration index was measured as SGC10 intensity normalized to the crush site. One way ANOVA. Sidak's multiple comparisons test *$p<0.05$.

(D) Representative images of dissociated DRG neurons from control and FasncKO, cultured for 20h, from naïve and injured (3 days post conditioning sciatic nerve injury) and stained with the neuronal marker Tuj1. n=8. Scale bar: 200 μm.

(E) Length of axons per neuron was measured. n=8, average of 500 neurons per replicate.

(F) Percentage of initiating neurons normalized to the total number of neurons was measured n=8, average of 500 neurons per replicate. Automated neurite tracing analysis using Nikon Elements. One way ANOVA. Sidak's multiple comparisons test *$p<0.05$ **$p<0.005$ ****$p<0.0001$.

Figure 6: Activation of PPARα in SGC promotes axon regeneration in co-cultures of neurons and SGC

(A) t-SNE overlay for expression of the genes PPARα, PPARγ, and PPARα target genes PPARGC1a, FADS2 and PEX11a .

(B) Heat map of PPARα target genes response to injury in SGC and neurons.

(C) Neuronal and axonal area in embryonic DRG spot co-culture at DIV7, immunostained for Fabp7 (green) and Tuj1 (red). Scale Bar: 100 μm (neuronal) and 50 μm (axonal).

(D) Embryonic DRG spot co-cultures axotomized at DIV7 after a 24 h pre-treatment with the indicated PPARα agonists at 2 concentrations (100nM and 10μM). Cultures were fixed after 24h and stained with SCG10. Scale Bar: 50 μm.

(E) Distance of regenerating axons was measured from the injury site. n=4 One way ANOVA Dunnett's multiple comparisons test. *p<0.05.

(F) Embryonic DRG spot neuronal culture was supplement with FDU (5-Flourouridine) to eliminate dividing cells in the culture. Axotomy was performed at DIV7 after a 24 h pre-treatment with the indicated PPARα agonists. Distance of regenerating axons was measured from injury site after 24h. n=4 One way ANOVA Dunnett's multiple comparisons test. Ns-non significant.

Figure 7: **Activation of PPARα in SGC promotes axon regeneration**

(A) qPCR analysis of PPARα target genes expression in DRG from mice fed with a normal diet vs. fenofibrate diet. n=3 One way ANOVA. Sidak's multiple comparisons test *p<0.05 **p<0.005 ***p<0.0005.

(B) Representative longitudinal sections of sciatic nerve from FasncKO mice fed with a normal diet or fenofibrate diet, stained for SCG10. Orange lines indicate the crush site. Scale Bar: 500 μm.

(C) Length of the longest 10 axons was measured in 10 sections for each nerve. n=8. One way ANOVA Sidak's multiple comparisons test ***p<0.0005 ns-non significant.

(D) Regeneration index was measured as SGC10 intensity normalized to the crush site. One way ANOVA. Sidak's multiple comparisons test *p<0.05.

(E) Representative images of dissociated DRG neurons from FasncKO mice fed with a normal diet or fenofibrate diet, cultured for 20h and stained with Tuj1. n=8. Scale bar: 200 μM.

(F) Length of axons per neuron was measured. n=8, average of 500 neurons per replicate.

(G) Percentage of initiating neurons out of total number of neurons was measured n=8, average of 500 neurons per replicate. Automated neurite tracing analysis using Nikon

Elements. One way ANOVA. Sidak's multiple comparisons test *p<0.05 **p<0.005 ns-non significant.

Supplementary Figures

Figure S1: Cluster analysis from scRNAseq of mouse DRG, **related to Figure 1**

(A) t-SNE overlaid for expression of marker genes for different cell populations including PECAM/DC31 for endothelial cells , AIF1/Iba-1 and CD68 for Macrophages. CD3G for T-cells, Isl1 for neurons, DES for smooth muscle cells, CD34 for mesenchymal cell and COL1A1 for connective tissue.

(B) Violin plots illustrate Schwann and SGC marker genes signatures of distinct cell populations.

(C) Top expressed genes in the SGC cluster (605 genes) was compared to top expressed genes in the Schwann cell cluster (572 genes)

(D) Top expressed genes in the SGC cluster (605 genes) was compared to the top expressed genes in astrocytes.

Figure S2: **Fabp7 is a specific marker for SGCs in adult mice DRG** , **related to Figure 2**

(A) DRG sections from Fabp7KO and control mice were immunostained for Fabp7 (green) and Tuj1 (red)

(B) DRG sections from Fabp7KO and control mice were for Glutamine Synthase (GS) (green) and Tuj1 (red). Scale bar: 50 µm

(C) Longitudinal sections of sciatic nerves from Fabp7KO and control mice immunostained for Fabp7 (green), Tuj1 (red) and Dapi. Scale bar: 50 µm.

(D) t-SNE plot of injured sciatic nerve (9 days post injury) analyzed from the single cell data (Carr et al., 2018). t-SNE overlay for the expression of PLP1 gene, indicating the Schwann cell cluster, and Fabp7.

Figure S3: Pathway analysis of differentially upregulated genes in major cell types**, related to Figure 3**

(A-F) Pathway analysis of differentially upregulated genes in major cell types in the DRG following nerve injury (KEGG 2016).

Figure S4: **Fatty Acid synthase deletion in SGC does not lead to neuronal cell death or abnormal functional properties, related to Figure 4**

(A) DRG sections from FasncKO and control mice in naïve and injured (3 days post injury) were immuonostained for Cleaved Caspase3 (green), Tuj1 (red) and Dapi (Blue). Scale bar: 50 µm.

(B) Whole-cell recordings in dissociated co-cultures of DRG neurons and glia. Medium diameter neurons (control 19.19 ± 0.42 µm, n = 16; FasncKO 19.27 ± 0.34 µm, n = 30, p = 0.88; that were associated with at least one glia cell were targeted for recordings.

(C) A subset of recorded cells was filled with biocytin (red) via the patch pipette for *post hoc* verification of neuronal identity; IB4- nociceptors (green) NF200- Proprioceptors/LTMRs (Cyan). Scale bar: 50 µm.

Figure S5: **Activation of PPARα in pure neuronal cultures does not enhance axon regeneration** , related to Figure 6

(A) Embryonic DRG were dissociated and plated as a spot with or without 5-fluorodeoxyuridine (FDU) and stained for Fabp7 (green), Tuj1 (red) and dapi (blue) at DIV6. n=5.

(B) Embryonic DRG spot co-culture, supplemented with FDU, were axotomized at DIV7 after a 24 h pre-treatment with the indicated PPARα agonists fenofibrate (10µM), Clifibrate (100nM) and GW7647 (10µM). Cultures were fixed after 24h and stained with SCG10. Scale Bar: 250 µm.

Supplementary Tables

Table 1: Top 10 expressed genes in each cell cluster

Table 2: Comparisons of genes expressed in Schwann cells, astrocytes and SGC

Table 3: Differentially expressed genes in SGC after nerve injury

Material and Methods

Animals and Procedures

All surgical procedures were completed as approved by Washington University in St. Louis School of Medicine Institutional Animal Care and Use Committee's regulations. During surgery, 8-12 week old C57Bl/6 mice or the indicate genotype were anesthetized using 2% inhaled isoflurane. For analgesia, 1mg/kg buprenorphine SR-LAB (ZooPharm) was administered subcutaneously. Sciatic nerve injuries were performed as previously described (Carlin et al., 2019; Cho et al., 2013) . Briefly, the sciatic nerve was exposed and crushed for 10 seconds using a #55 forceps. The wound was closed using wound clips and both injured dorsal root ganglia and sciatic nerve were dissected at the indicated time post-surgery. Contralateral nerve and DRG served as uninjured controls, when needed. Tamoxifen (500mg per kg diet, TD.130858) and Fenofibrate (0.2%, Sigma Cat# F6020) were administrated as chow pellets (Envigo Tekland).

Mouse strains

Male and female mice were used for all experiments. 8-10 weeks old -12 week old C57Bl/6 were used. *Rosa26-ZsGreen* (also known as Ai6(RCL-ZsGreen) was obtained from Jackson RRID:IMSR_JAX:007906; (Madisen et al., 2010). Fabp7KO mouse line was a generous gift from Dr. Owada (Owada et al., 2006). The Sunf1GFP mice (Gt(ROSA)26Sortm5(CAG-Sun1/sfGFP)Nat) was a generous gift from Dr. Harrison Gabel. mice carrying floxed *Fasn* alleles were previously generated (Chakravarthy et al., 2005). The BLBP-cre ER mouse line (Maruoka et al., 2011) was a generous gift from Dr. Toshihiko Hosoya.

Single cell RNAseq

L4 and L5 DRG's from mice 8-12 weeks old were collected into cold Hank's balanced salt solution (HBSS) with 5% Hepes, then transferred to warm Papain solution and incubated for 20 min in 37ºC. DRG's were washed in HBSS and incubated with Collagenase for 20 min in 37ºC. Ganglia were then mechanically dissociated to a single cell suspension by triturating in culture medium (Neurobasal medium), with Glutamax, PenStrep and B-27. Cells were washed in HBSS+Hepes +0.1%BSA solution, passed through a 70-micron cell strainer. Hoechst dye was added to distinguish live cells from debris and cells were FACS sorted using MoFlo HTS with Cyclone (Beckman Coulter, Indianapolis, IN). Sorted cells were washed in HBSS+Hepes+0.1%BSA solution and manually counted using hemocytometer. Solution was adjusted to a concentration of 500cell/microliter and loaded on the 10X Chromium system. Single-cell RNA-Seq libraries were prepared using GemCode Single-Cell 3′ Gel Bead and Library Kit (10x Genomics). A digital expression matrix was obtained using 10X's CellRanger pipeline (Washington University Genome Technology Access Center). Quantification and statistical analysis were done with Partek Flow package.

Data Deposition

The Fastq files for scRNA sequencing were deposited at the NCBI GEO database under the accession number GSE139103.

Tissue Preparation and Immunohistochemistry

After isolation of either sciatic nerve or DRG, tissue was fixed using 4% paraformaldehyde for 1 hour at room temperature. Tissue was then washed in PBS and cryoprotected using 30% sucrose solution at 4C overnight. Next, the tissue was embedded in O.C.T., frozen, and mounted for cryosectioning. All frozen sections were cut to a width of 12μm for subsequent staining. For immunostaining of DRG and nerve sections, slides were washed 3x in PBS and then blocked for in solution containing 10% goat serum in .2% Triton-PBS for 1 hour. Next, sections were incubated overnight in blocking solution containing primary antibody. The next day, sections were washed

3x with PBS and then incubated in blocking solution containing a secondary antibody for 1 hour at room temperature. Finally, sections were washed 3x with PBS and mounted using ProLong Gold antifade (Thermo Fisher Scientific). Images were acquired at 10x or 20x using a Nikon TE2000E inverted microscope and images were analyzed using Nikon Elements. Antibodies were as follow: SCG10/Stmn2 (1:1000; Novus catalog #NBP1-49461, RRID:AB_10011569), Tubb3/βIII tubulin antibody (BioLegend catalog #802001, RRID:AB_291637), *Griffonia simplicifolia* isolectin B4 (IB4) directly conjugated to Alexa Fluor 488 or Alexa Fluor 594 (Thermo Fisher Scientific catalog #I21411 and #I21413), Fabp7 (Thermo Fisher Scientific Cat# PA5-24949, RRID:AB_2542449), cleaved caspase 3 (CST Cat# 9664, RRID:AB_2070042), Fasn (Abcam, Catalog #ab128870), Glutamine synthase (Abcam, Catalog #ab49873).

DRG Cultures and Regeneration Assays

For in vitro regeneration assay, dorsal root ganglia were isolated from time pregnant e13.5 CD-1 mice and cultured as previously described (Cho et al., 2013; Oh et al., 2018). Briefly, after a short centrifugation, dissection media was aspirated and cells were digested in .05% Trypsin-EDTA for 25 minutes in 37°C. Next, cells were pelleted by centrifuging for 2 minutes at 500 x g, the supernatant was aspirated, and Neurobasal was added. Cells were then triturated 25x and added to the growth medium containing Neurobasal media, B27 Plus, 1ng/ml NGF, Glutamax and Pen/Strep, with or without 5μM 5-deoxyfluoruridine (FDU). Approximately 10,000 cells were added to each well in a 2.5 μl spot. Spotted cells were allowed to adhere for 10 minutes before the addition of the growth medium. Plates were pre-coated with 100ug/ml poly-D-lysine. For regeneration assays, PPARα agonists were added to the culture on DIV6. Cells were then injured using an 8mm microtome blade on DIV7 and fixed 24h later. Cells were washed with PBS and stained for SCG10 as described above.

For adult DRG cultures DRG were dissected from naïve mice. Cells were prepared as described above for single cell protocol and cultured on 100ug/ml poly-D-lysine coated plates and fixed 20h later. Cultures were then used for electrophysiological recording 24h after plating or fixed and stained with the indicated antibody. Images were acquired at 10x using a Nikon TE2000 microscope and image analysis was completed using Nikon Elements.

Image Analysis

For sciatic nerve injury experiments, images were quantified in two ways. First, the injury site was defined as the area with maximal SCG10 intensity. A vertical line was drawn across this region and the longest 10 axons were measured from that site and the average length reported (Carlin et al., 2019). Next, SCG10 intensity was quantified at 1, 2, and 3mm from the injury site as previously described (Cho et al., 2015; Cho et al., 2013). The intensity was normalized to the injury site and the percent intensity was reported. For both quantifications, five sections per biological replicate were averaged.

For embryonic dorsal root ganglia experiments, regenerative length was measured from the visible blade mark to the end of the regenerating axons. Each technical replicate was measured 4-6 times and three technical replicates were measured per biological replicate.

To determine the cleaved caspase staining area, a binary was generated to fit the positive signal, and positive staining area was measured. That area was internally normalized to Dapi positive staining area.

RNA Isolation and Quantitative PCR

DRG and nerves were lysed and total RNA was extracted using Trizol reagent (Thermo Fisher, Cat# 15596026).). Next, RNA concentration was determined using a NanoDrop 2000 (Thermo Fisher Scientific). First strand synthesis was then performed using the High Capacity cDNA Reverse Transcription kit (Applied Biosystems). Quantitative PCR was performed using

PowerUp SYBR Green master mix (Thermo Fisher, Cat# a25742) using 5ng of cDNA per reaction. Plates were run on a QuantStudio 6 Flex and analyzed in Microsoft Excel. The average Ct value from three technical replicates was averaged normalized to the internal control Rpl13a. All primer sequences were obtained from PrimerBank (Spandidos et al., 2010) and product size validated using agarose gel electrophoresis.

Ppara (PrimerBank ID 31543500a1) Forward Primer AGAGCCCCATCTGTCCTCTC

Reverse Primer ACTGGTAGTCTGCAAAACCAAA

Pex11a (PrimerBank ID 6755034a1) Forward Primer GACGCCTTCATCCGAGTCG Reverse Primer CGGCCTCTTTGTCAGCTTTAGA.

Fads2 (PrimerBank ID 9790070c1) Forward Primer TCATCGGACACTATTCGGGAG Reverse Primer GGGCCAGCTCACCAATCAG.

Hmgcs1 (PrimerBank ID 31981842a1) Forward Primer AACTGGTGCAGAAATCTCTAGC Reverse Primer GGTTGAATAGCTCAGAACTAGCC

ApoE (PrimerBank ID 6753102a1) Forward Primer CTGACAGGATGCCTAGCCG Reverse Primer CGCAGGTAATCCCAGAAGC

Electrophoresis and western blot

DRG and sciatic nerve samples were lysed in 5× SDS loading buffer, heated at 95 °C for 5 min and were run in on 8–16% NuPAGE SDS-PAGE gradient gel (Life Technologies) in MOPS SDS Running Buffer (Life Technologies) and transferred to 0.45 μm nitrocellulose membranes (Amersham). Next, these membranes were blocked in blocking buffer (3% BSA in 0.1% Tween-20 at pH 7.6 for 1 h, and incubated at 4 °C overnight in blocking buffer with primary antibodies. Membranes were then washed in TBST 3 times, incubated with horseradish peroxidase (HRP)-conjugated anti-rabbit or anti-mouse IgG (Invitrogen) for 1 h at room temperature, washed in TBST three times, and developed with SuperSignal West Dura Chemiluminescent Substrate

(Thermo Scientific). The membranes were imaged using ChemiDoc System (Bio Rad) and analyzed with ImageLab software. For quantification, Fasn intensity was normalized to loading control Gapdh (Santa Cruz, catalog# sc25778)

Whole-cell electrophysiology

Whole-cell patch-clamp recordings in a current-clamp mode were performed using a Multiclamp 700B amplifier (Molecular Devices) from acutely isolated DRG neurons visually identified with infrared video microscopy and differential interference contrast optics (Olympus BX51WI). Current-clamp recordings were made with pipette capacitance compensation and bridge-balance compensation. Recordings were conducted at near-physiological temperature (33–34°C). The recording electrodes were filled with the following (in mM): 130 K-gluconate, 10 KCl, 0.1 EGTA, 2 $MgCl_2$, 2 $ATPNa_2$, 0.4 GTPNa, and 10 HEPES, pH 7.3. The extracellular solution contained (in mM): 145 NaCl, 3 KCl, 10 HEPES, 2.5 $CaCl_2$, 1.2 $MgCl_2$, and 7 glucose, pH 7.4 (saturated with 95% O_2 and 5% CO_2). For determination of action potential (AP) threshold, APs were evoked by a ramp current injection (0.1 pA/ms) (Deng and Klyachko, 2016; Yamada-Hanff and Bean, 2013) with a hyperpolarizing onset to ensure maximal Na^+ channel availability before the first AP. The AP thresholds were determined only from the first APs of ramp-evoked AP trains. AP threshold (i.e., threshold voltage) was defined as the voltage at the voltage trace turning point, corresponding to the first peak of 3rd order derivative of AP trace (Deng and Klyachko, 2016; Lu et al., 2012). Data were averaged over 5-8 trials for each cell. Resting membrane potential (RMP) was measured immediately after whole-cell formation. Cell capacitance was determined by the amplifier's auto whole-cell compensation function with slight manual adjustment to optimize the measurement if needed. Under current-clamp mode, a negative current (−50 pA for 500 ms) was injected every 5 s to assess the input resistance.

TEM

Mice were perfused with 2.5% glutaraldehyde with 4% paraformaldehyde in 0.1M Cacodylate buffer, followed by post fix. A secondary fix was done with 1% osmium tetroxide. For Transmission electron microscopy (TEM), tissue was dehydrated with ethanol and embedded with spurr's resin. Thin sections (70 nm) were mounted on mesh grids and stained with 8% uranyl acetate followed by Sato's lead stain. Sections were imaged on a Jeol (JEM-1400) electron microscope and acquired with an AMT V601 digital camera. (Washington University Center for Cellular Imaging).

Quantification and statistical analysis

Quantifications were performed by a blinded experimenter to genotype and treatment. Fiji (ImageJ) analysis software was used to measure TEM nerve images. NIkon Elements analysis software was used to trace regenerating axon in nerve sections and in the embryonic DRG spot culture. An Automated analysis for axon tracing and neurons soma count was used for ex-vivo adult DRG culture experiments (Nikon elements). Statistics was performed using GraphPad (Prism8) for either Student's t-test or ANOVA analysis. Error bars indicate the standard error of the mean (SEM).

References

Almad, A., Lash, A.T., Wei, P., Lovett-Racke, A.E., and McTigue, D.M. (2011). The PPAR alpha agonist gemfibrozil is an ineffective treatment for spinal cord injured mice. Experimental neurology *232*, 309-317.

Barres, B.A., and Smith, S.J. (2001). Neurobiology. Cholesterol--making or breaking the synapse. Science *294*, 1296-1297.

Blom, C.L., Martensson, L.B., and Dahlin, L.B. (2014). Nerve injury-induced c-Jun activation in Schwann cells is JNK independent. Biomed Res Int *2014*, 392971.

Bogdanov, P., Hernandez, C., Corraliza, L., Carvalho, A.R., and Simo, R. (2015). Effect of fenofibrate on retinal neurodegeneration in an experimental model of type 2 diabetes. Acta Diabetol *52*, 113-122.

Britsch, S., Goerich, D.E., Riethmacher, D., Peirano, R.I., Rossner, M., Nave, K.A., Birchmeier, C., and Wegner, M. (2001). The transcription factor Sox10 is a key regulator of peripheral glial development. Genes Dev *15*, 66-78.

Carlin, D., Halevi, A.E., Ewan, E.E., Moore, A.M., and Cavalli, V. (2019). Nociceptor Deletion of Tsc2 Enhances Axon Regeneration by Inducing a Conditioning Injury Response in Dorsal Root Ganglia. eNeuro *6*.

Carr, M.J., Toma, J.S., Johnston, A.P.W., Steadman, P.E., Yuzwa, S.A., Mahmud, N., Frankland, P.W., Kaplan, D.R., and Miller, F.D. (2019). Mesenchymal Precursor Cells in Adult Nerves Contribute to Mammalian Tissue Repair and Regeneration. Cell stem cell *24*, 240-256 e249.

Chakravarthy, M.V., Lodhi, I.J., Yin, L., Malapaka, R.R., Xu, H.E., Turk, J., and Semenkovich, C.F. (2009). Identification of a physiologically relevant endogenous ligand for PPARalpha in liver. Cell *138*, 476-488.

Chakravarthy, M.V., Pan, Z., Zhu, Y., Tordjman, K., Schneider, J.G., Coleman, T., Turk, J., and Semenkovich, C.F. (2005). "New" hepatic fat activates PPARalpha to maintain glucose, lipid, and cholesterol homeostasis. Cell Metab *1*, 309-322.

Chen, X.R., Besson, V.C., Palmier, B., Garcia, Y., Plotkine, M., and Marchand-Leroux, C. (2007a). Neurological recovery-promoting, anti-inflammatory, and anti-oxidative effects afforded by fenofibrate, a PPAR alpha agonist, in traumatic brain injury. J Neurotrauma *24*, 1119-1131.

Chen, Y., Li, G., and Huang, L.Y. (2015). p38 MAPK mediates glial P2X7R-neuronal P2Y1R inhibitory control of P2X3R expression in dorsal root ganglion neurons. Molecular pain *11*, 68.

Chen, Z.L., Yu, W.M., and Strickland, S. (2007b). Peripheral regeneration. Annu Rev Neurosci *30*, 209-233.

Cherkas, P.S., Huang, T.Y., Pannicke, T., Tal, M., Reichenbach, A., and Hanani, M. (2004). The effects of axotomy on neurons and satellite glial cells in mouse trigeminal ganglion. Pain *110*, 290-298.

Cho, Y., and Cavalli, V. (2012). HDAC5 is a novel injury-regulated tubulin deacetylase controlling axon regeneration. EMBO J *31*, 3063-3078.

Cho, Y., Shin, J.E., Ewan, E.E., Oh, Y.M., Pita-Thomas, W., and Cavalli, V. (2015). Activating Injury-Responsive Genes with Hypoxia Enhances Axon Regeneration through Neuronal HIF-1alpha. Neuron *88*, 720-734.

Cho, Y., Sloutsky, R., Naegle, K.M., and Cavalli, V. (2013). Injury-induced HDAC5 nuclear export is essential for axon regeneration. Cell *155*, 894-908.

Christie, K., Koshy, D., Cheng, C., Guo, G., Martinez, J.A., Duraikannu, A., and Zochodne, D.W. (2015). Intraganglionic interactions between satellite cells and adult sensory neurons. Mol Cell Neurosci *67*, 1-12.
Dean, J.M., and Lodhi, I.J. (2018). Structural and functional roles of ether lipids. Protein Cell *9*, 196-206.
Deng, P.Y., and Klyachko, V.A. (2016). Increased Persistent Sodium Current Causes Neuronal Hyperexcitability in the Entorhinal Cortex of Fmr1 Knockout Mice. Cell Rep *16*, 3157-3166.
Donegan, M., Kernisant, M., Cua, C., Jasmin, L., and Ohara, P.T. (2013). Satellite glial cell proliferation in the trigeminal ganglia after chronic constriction injury of the infraorbital nerve. Glia *61*, 2000-2008.
Ebrahimi, M., Yamamoto, Y., Sharifi, K., Kida, H., Kagawa, Y., Yasumoto, Y., Islam, A., Miyazaki, H., Shimamoto, C., Maekawa, M.*, et al.* (2016). Astrocyte-expressed FABP7 regulates dendritic morphology and excitatory synaptic function of cortical neurons. Glia *64*, 48-62.
Feng, L., Hatten, M.E., and Heintz, N. (1994). Brain lipid-binding protein (BLBP): a novel signaling system in the developing mammalian CNS. Neuron *12*, 895-908.
Fenzi, F., Benedetti, M.D., Moretto, G., and Rizzuto, N. (2001). Glial cell and macrophage reactions in rat spinal ganglion after peripheral nerve lesions: an immunocytochemical and morphometric study. Archives italiennes de biologie *139*, 357-365.
Furuhashi, M., and Hotamisligil, G.S. (2008). Fatty acid-binding proteins: role in metabolic diseases and potential as drug targets. Nat Rev Drug Discov *7*, 489-503.
George, D., Ahrens, P., and Lambert, S. (2018). Satellite glial cells represent a population of developmentally arrested Schwann cells. Glia.
Hanani, M. (2005). Satellite glial cells in sensory ganglia: from form to function. Brain Res Brain Res Rev *48*, 457-476.
Hanani, M. (2015). Role of satellite glial cells in gastrointestinal pain. Front Cell Neurosci *9*, 412.
Hanani, M., Huang, T.Y., Cherkas, P.S., Ledda, M., and Pannese, E. (2002). Glial cell plasticity in sensory ganglia induced by nerve damage. Neuroscience *114*, 279-283.
He, Z., and Jin, Y. (2016). Intrinsic Control of Axon Regeneration. Neuron *90*, 437-451.
Holland, S.D., Ramer, L.M., McMahon, S.B., Denk, F., and Ramer, M.S. (2019). An ATF3-CreERT2 Knock-In Mouse for Axotomy-Induced Genetic Editing: Proof of Principle. eNeuro *6*.
Huang, L.Y., Gu, Y., and Chen, Y. (2013). Communication between neuronal somata and satellite glial cells in sensory ganglia. Glia *61*, 1571-1581.
Huang, T.Y., Belzer, V., and Hanani, M. (2010). Gap junctions in dorsal root ganglia: possible contribution to visceral pain. European journal of pain *14*, 49 e41-11.
Huang, T.Y., Cherkas, P.S., Rosenthal, D.W., and Hanani, M. (2005). Dye coupling among satellite glial cells in mammalian dorsal root ganglia. Brain research *1036*, 42-49.
Jager, S.B., Pallesen, L.T., and Vaegter, C.B. (2018). Isolation of satellite glial cells for high-quality RNA purification. J Neurosci Methods *297*, 1-8.
Jasmin, L., Vit, J.P., Bhargava, A., and Ohara, P.T. (2010). Can satellite glial cells be therapeutic targets for pain control? Neuron glia biology *6*, 63-71.
Jessen, K.R., and Mirsky, R. (2016). The repair Schwann cell and its function in regenerating nerves. J Physiol *594*, 3521-3531.
Kastriti, M.E., and Adameyko, I. (2017). Specification, plasticity and evolutionary origin of peripheral glial cells. Current opinion in neurobiology *47*, 196-202.

Kim, E.N., Lim, J.H., Kim, M.Y., Kim, H.W., Park, C.W., Chang, Y.S., and Choi, B.S. (2016a). PPARalpha agonist, fenofibrate, ameliorates age-related renal injury. Exp Gerontol *81*, 42-50.
Kim, Y.S., Anderson, M., Park, K., Zheng, Q., Agarwal, A., Gong, C., Saijilafu, Young, L., He, S., LaVinka, P.C*., et al.* (2016b). Coupled Activation of Primary Sensory Neurons Contributes to Chronic Pain. Neuron *91*, 1085-1096.
Krishnan, A., Bhavanam, S., and Zochodne, D. (2018). An Intimate Role for Adult Dorsal Root Ganglia Resident Cycling Cells in the Generation of Local Macrophages and Satellite Glial Cells. J Neuropathol Exp Neurol *77*, 929-941.
Kung, L.H., Gong, K., Adedoyin, M., Ng, J., Bhargava, A., Ohara, P.T., and Jasmin, L. (2013). Evidence for glutamate as a neuroglial transmitter within sensory ganglia. PloS one *8*, e68312.
Kurtz, A., Zimmer, A., Schnutgen, F., Bruning, G., Spener, F., and Muller, T. (1994). The expression pattern of a novel gene encoding brain-fatty acid binding protein correlates with neuronal and glial cell development. Development *120*, 2637-2649.
LeBlanc, A.C., and Poduslo, J.F. (1990). Regulation of apolipoprotein E gene expression after injury of the rat sciatic nerve. J Neurosci Res *25*, 162-171.
Ledda, M., De Palo, S., and Pannese, E. (2004). Ratios between number of neuroglial cells and number and volume of nerve cells in the spinal ganglia of two species of reptiles and three species of mammals. Tissue Cell *36*, 55-62.
Lee, C.H., Olson, P., and Evans, R.M. (2003). Minireview: lipid metabolism, metabolic diseases, and peroxisome proliferator-activated receptors. Endocrinology *144*, 2201-2207.
Lezana, J.P., Dagan, S.Y., Robinson, A., Goldstein, R.S., Fainzilber, M., Bronfman, F.C., and Bronfman, M. (2016). Axonal PPARgamma promotes neuronal regeneration after injury. Dev Neurobiol *76*, 688-701.
Li, F.Q., Fowler, K.A., Neil, J.E., Colton, C.A., and Vitek, M.P. (2010). An apolipoprotein E-mimetic stimulates axonal regeneration and remyelination after peripheral nerve injury. J Pharmacol Exp Ther *334*, 106-115.
Lodhi, I.J., Yin, L., Jensen-Urstad, A.P., Funai, K., Coleman, T., Baird, J.H., El Ramahi, M.K., Razani, B., Song, H., Fu-Hsu, F*., et al.* (2012). Inhibiting adipose tissue lipogenesis reprograms thermogenesis and PPARgamma activation to decrease diet-induced obesity. Cell Metab *16*, 189-201.
Lu, U., Roach, S.M., Song, D., and Berger, T.W. (2012). Nonlinear dynamic modeling of neuron action potential threshold during synaptically driven broadband intracellular activity. IEEE Trans Biomed Eng *59*, 706-716.
Madisen, L., Zwingman, T.A., Sunkin, S.M., Oh, S.W., Zariwala, H.A., Gu, H., Ng, L.L., Palmiter, R.D., Hawrylycz, M.J., Jones, A.R*., et al.* (2010). A robust and high-throughput Cre reporting and characterization system for the whole mouse brain. Nature neuroscience *13*, 133-140.
Mahar, M., and Cavalli, V. (2018). Intrinsic mechanisms of neuronal axon regeneration. Nat Rev Neurosci *19*, 323-337.
Maruoka, H., Kubota, K., Kurokawa, R., Tsuruno, S., and Hosoya, T. (2011). Periodic organization of a major subtype of pyramidal neurons in neocortical layer V. The Journal of neuroscience : the official journal of the Society for Neuroscience *31*, 18522-18542.
Matsumata, M., Inada, H., and Osumi, N. (2016). Fatty acid binding proteins and the nervous system: Their impact on mental conditions. Neurosci Res *102*, 47-55.

Matsumata, M., Sakayori, N., Maekawa, M., Owada, Y., Yoshikawa, T., and Osumi, N. (2012). The effects of Fabp7 and Fabp5 on postnatal hippocampal neurogenesis in the mouse. Stem Cells *30*, 1532-1543.
Miller, K.E., Richards, B.A., and Kriebel, R.M. (2002). Glutamine-, glutamine synthetase-, glutamate dehydrogenase- and pyruvate carboxylase-immunoreactivities in the rat dorsal root ganglion and peripheral nerve. Brain research *945*, 202-211.
Miller, S.J., Li, H., Rizvi, T.A., Huang, Y., Johansson, G., Bowersock, J., Sidani, A., Vitullo, J., Vogel, K., Parysek, L.M.*, et al.* (2003). Brain lipid binding protein in axon-Schwann cell interactions and peripheral nerve tumorigenesis. Mol Cell Biol *23*, 2213-2224.
Mo, A., Mukamel, E.A., Davis, F.P., Luo, C., Henry, G.L., Picard, S., Urich, M.A., Nery, J.R., Sejnowski, T.J., Lister, R.*, et al.* (2015). Epigenomic Signatures of Neuronal Diversity in the Mammalian Brain. Neuron *86*, 1369-1384.
Montani, L., Pereira, J.A., Norrmen, C., Pohl, H.B.F., Tinelli, E., Trotzmuller, M., Figlia, G., Dimas, P., von Niederhausern, B., Schwager, R.*, et al.* (2018). De novo fatty acid synthesis by Schwann cells is essential for peripheral nervous system myelination. The Journal of cell biology *217*, 1353-1368.
Moreno, S., and Ceru, M.P. (2015). In search for novel strategies towards neuroprotection and neuroregeneration: is PPARalpha a promising therapeutic target? Neural Regen Res *10*, 1409-1412.
Obata, K., Yamanaka, H., Dai, Y., Mizushima, T., Fukuoka, T., Tokunaga, A., and Noguchi, K. (2004). Differential activation of MAPK in injured and uninjured DRG neurons following chronic constriction injury of the sciatic nerve in rats. The European journal of neuroscience *20*, 2881-2895.
Oh, Y.M., Mahar, M., Ewan, E.E., Leahy, K.M., Zhao, G., and Cavalli, V. (2018). Epigenetic regulator UHRF1 inactivates REST and growth suppressor gene expression via DNA methylation to promote axon regeneration. Proceedings of the National Academy of Sciences of the United States of America *115*, E12417-E12426.
Owada, Y., Abdelwahab, S.A., Kitanaka, N., Sakagami, H., Takano, H., Sugitani, Y., Sugawara, M., Kawashima, H., Kiso, Y., Mobarakeh, J.I.*, et al.* (2006). Altered emotional behavioral responses in mice lacking brain-type fatty acid-binding protein gene. The European journal of neuroscience *24*, 175-187.
Pannese, E. (1964). Number and Structure of Perisomatic Satellite Cells of Spinal Ganglia under Normal Conditions or during Axon Regeneration and Neuronal Hypertrophy. Zeitschrift fur Zellforschung und mikroskopische Anatomie *63*, 568-592.
Pannese, E. (1981). The satellite cells of the sensory ganglia. Advances in anatomy, embryology, and cell biology *65*, 1-111.
Pannese, E. (2010). The structure of the perineuronal sheath of satellite glial cells (SGCs) in sensory ganglia. Neuron glia biology *6*, 3-10.
Rakhshandehroo, M., Knoch, B., Muller, M., and Kersten, S. (2010). Peroxisome proliferator-activated receptor alpha target genes. PPAR Res *2010*.
Rosenson, R.S. (2008). Fenofibrate: treatment of hyperlipidemia and beyond. Expert Rev Cardiovasc Ther *6*, 1319-1330.

Sharifi, K., Morihiro, Y., Maekawa, M., Yasumoto, Y., Hoshi, H., Adachi, Y., Sawada, T., Tokuda, N., Kondo, H., Yoshikawa, T.*, et al.* (2011). FABP7 expression in normal and stab-injured brain cortex and its role in astrocyte proliferation. Histochem Cell Biol *136*, 501-513.
Shin, J.E., Geisler, S., and DiAntonio, A. (2014). Dynamic regulation of SCG10 in regenerating axons after injury. Experimental neurology *252*, 1-11.
Shin, J.E., Ha, H., Cho, E.H., Kim, Y.K., and Cho, Y. (2018). Comparative analysis of the transcriptome of injured nerve segments reveals spatiotemporal responses to neural damage in mice. J Comp Neurol *526*, 1195-1208.
Smith, D.S., and Skene, J.H. (1997). A transcription-dependent switch controls competence of adult neurons for distinct modes of axon growth. The Journal of neuroscience : the official journal of the Society for Neuroscience *17*, 646-658.
Snipes, G.J., McGuire, C.B., Norden, J.J., and Freeman, J.A. (1986). Nerve injury stimulates the secretion of apolipoprotein E by nonneuronal cells. Proceedings of the National Academy of Sciences of the United States of America *83*, 1130-1134.
Spandidos, A., Wang, X., Wang, H., and Seed, B. (2010). PrimerBank: a resource of human and mouse PCR primer pairs for gene expression detection and quantification. Nucleic acids research *38*, D792-799.
Stephenson, J.L., and Byers, M.R. (1995). GFAP immunoreactivity in trigeminal ganglion satellite cells after tooth injury in rats. Experimental neurology *131*, 11-22.
Suadicani, S.O., Cherkas, P.S., Zuckerman, J., Smith, D.N., Spray, D.C., and Hanani, M. (2010). Bidirectional calcium signaling between satellite glial cells and neurons in cultured mouse trigeminal ganglia. Neuron glia biology *6*, 43-51.
van Deijk, A.F., Camargo, N., Timmerman, J., Heistek, T., Brouwers, J.F., Mogavero, F., Mansvelder, H.D., Smit, A.B., and Verheijen, M.H. (2017). Astrocyte lipid metabolism is critical for synapse development and function in vivo. Glia *65*, 670-682.
Vance, J.E., Campenot, R.B., and Vance, D.E. (2000). The synthesis and transport of lipids for axonal growth and nerve regeneration. Biochim Biophys Acta *1486*, 84-96.
Vance, J.E., Pan, D., Campenot, R.B., Bussiere, M., and Vance, D.E. (1994). Evidence that the major membrane lipids, except cholesterol, are made in axons of cultured rat sympathetic neurons. J Neurochem *62*, 329-337.
Varga, T., Czimmerer, Z., and Nagy, L. (2011). PPARs are a unique set of fatty acid regulated transcription factors controlling both lipid metabolism and inflammation. Biochim Biophys Acta *1812*, 1007-1022.
Vit, J.P., Jasmin, L., Bhargava, A., and Ohara, P.T. (2006). Satellite glial cells in the trigeminal ganglion as a determinant of orofacial neuropathic pain. Neuron glia biology *2*, 247-257.
Vit, J.P., Ohara, P.T., Bhargava, A., Kelley, K., and Jasmin, L. (2008). Silencing the Kir4.1 potassium channel subunit in satellite glial cells of the rat trigeminal ganglion results in pain-like behavior in the absence of nerve injury. The Journal of neuroscience : the official journal of the Society for Neuroscience *28*, 4161-4171.
Warwick, R.A., and Hanani, M. (2013). The contribution of satellite glial cells to chemotherapy-induced neuropathic pain. European journal of pain *17*, 571-580.
Weider, M., Wegener, A., Schmitt, C., Kuspert, M., Hillgartner, S., Bosl, M.R., Hermans-Borgmeyer, I., Nait-Oumesmar, B., and Wegner, M. (2015). Elevated in vivo levels of a single

transcription factor directly convert satellite glia into oligodendrocyte-like cells. PLoS Genet *11*, e1005008.
Xie, W., Strong, J.A., and Zhang, J.M. (2009). Early blockade of injured primary sensory afferents reduces glial cell activation in two rat neuropathic pain models. Neuroscience *160*, 847-857.
Xu, M., Aita, M., and Chavkin, C. (2008). Partial infraorbital nerve ligation as a model of trigeminal nerve injury in the mouse: behavioral, neural, and glial reactions. The journal of pain : official journal of the American Pain Society *9*, 1036-1048.
Yamada-Hanff, J., and Bean, B.P. (2013). Persistent sodium current drives conditional pacemaking in CA1 pyramidal neurons under muscarinic stimulation. J Neurosci *33*, 15011-15021.
Zhang, H., Mei, X., Zhang, P., Ma, C., White, F.A., Donnelly, D.F., and Lamotte, R.H. (2009). Altered functional properties of satellite glial cells in compressed spinal ganglia. Glia *57*, 1588-1599.
Zhang, X., Chen, Y., Wang, C., and Huang, L.Y. (2007). Neuronal somatic ATP release triggers neuron-satellite glial cell communication in dorsal root ganglia. Proceedings of the National Academy of Sciences of the United States of America *104*, 9864-9869.
Zhang, X.F., Han, P., Faltynek, C.R., Jarvis, M.F., and Shieh, C.C. (2005). Functional expression of P2X7 receptors in non-neuronal cells of rat dorsal root ganglia. Brain research *1052*, 63-70.
Zhang, Y., Chen, K., Sloan, S.A., Bennett, M.L., Scholze, A.R., O'Keeffe, S., Phatnani, H.P., Guarnieri, P., Caneda, C., Ruderisch, N.*, et al.* (2014). An RNA-sequencing transcriptome and splicing database of glia, neurons, and vascular cells of the cerebral cortex. The Journal of neuroscience : the official journal of the Society for Neuroscience *34*, 11929-11947.
Zhou, X.F., Rush, R.A., and McLachlan, E.M. (1996). Differential expression of the p75 nerve growth factor receptor in glia and neurons of the rat dorsal root ganglia after peripheral nerve transection. The Journal of neuroscience : the official journal of the Society for Neuroscience *16*, 2901-2911.

Fig.1

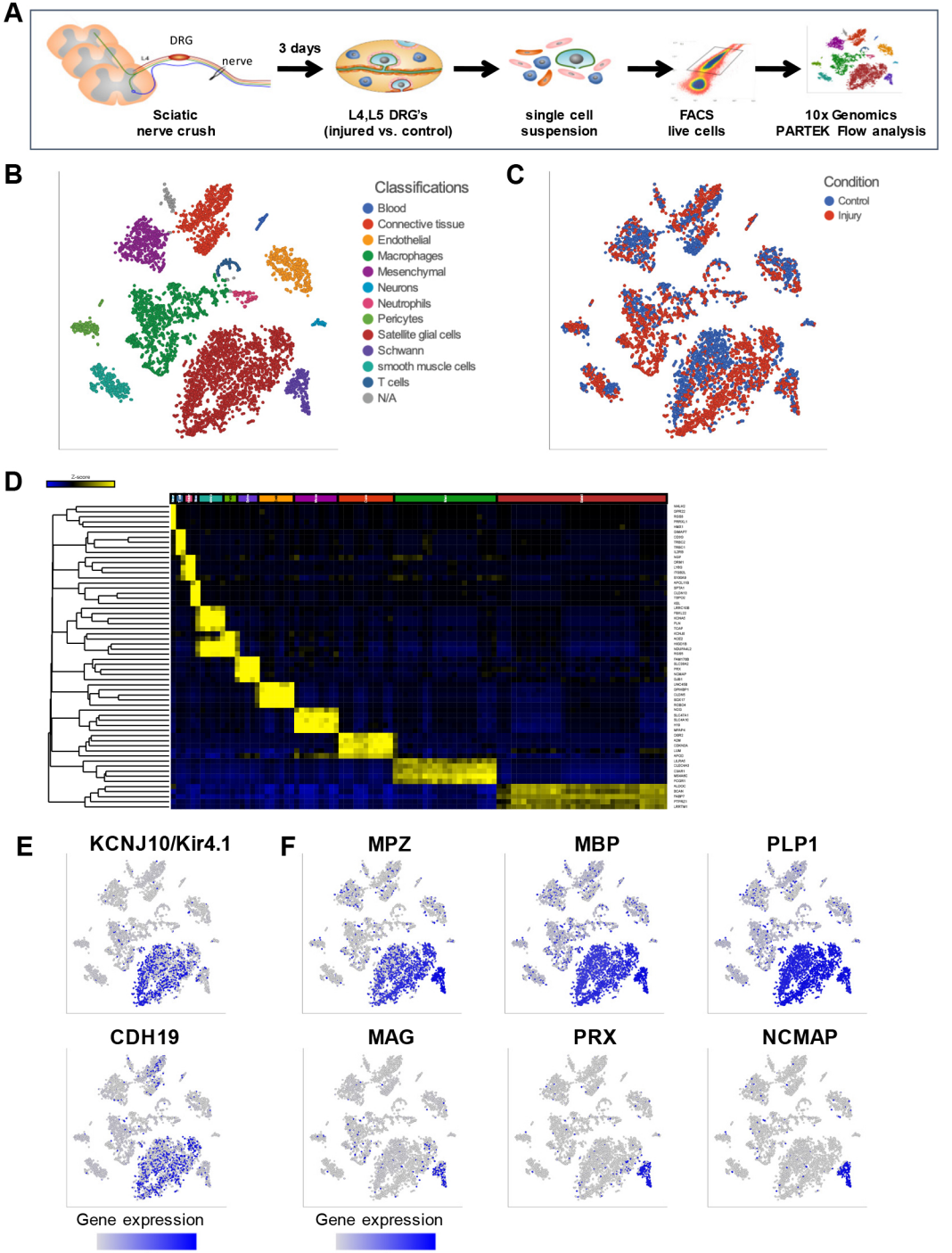
A
DRG
L4
nerve
3 days
Sciatic nerve crush
L4,L5 DRG's (injured vs. control)
single cell suspension
FACS live cells
10x Genomics PARTEK Flow analysis
B
Classifications
Blood
Connective tissue
Endothelial
Macrophages
Mesenchymal
Neurons
Neutrophils
Pericytes
Satellite glial cells
Schwann
smooth muscle cells
T cells
N/A
C
Condition
Control
Injury
D
Z-score
E
KCNJ10/Kir4.1
F
MPZ
MBP
PLP1
CDH19
MAG
PRX
NCMAP
Gene expression
Gene expression

Fig.S1

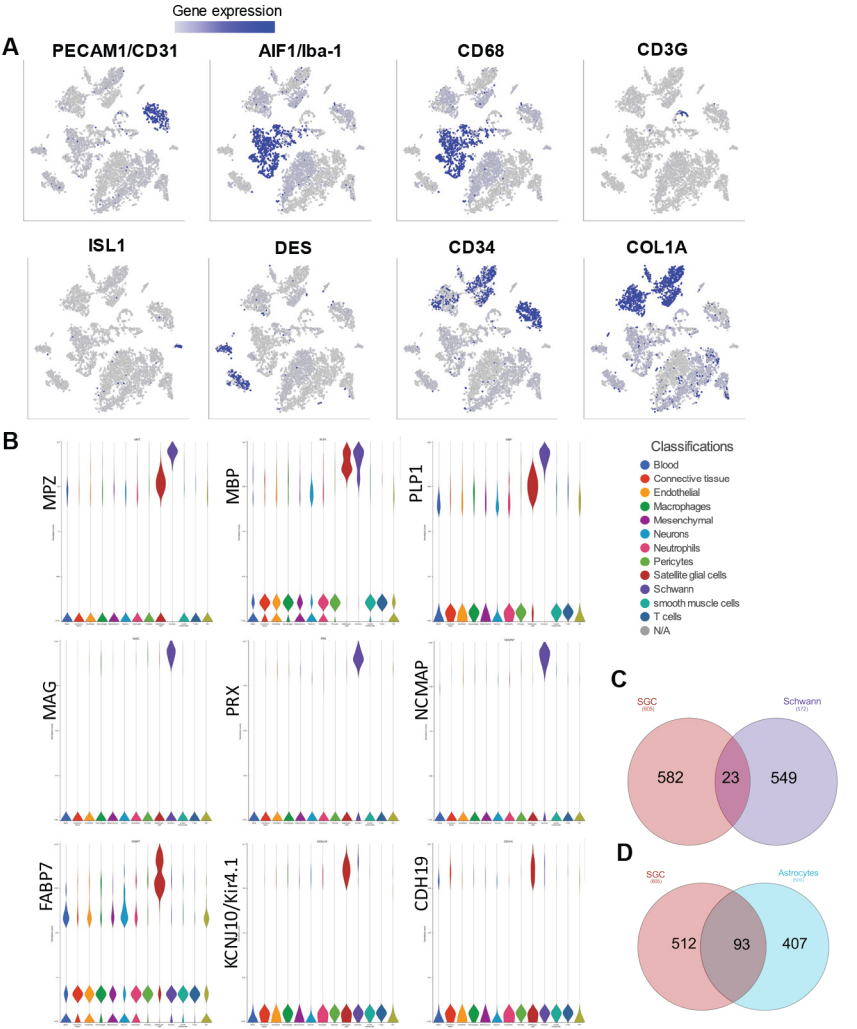
Gene expression
A
PECAM1/CD31
AIF1/Iba-1
CD68
CD3G
ISL1
DES
CD34
COL1A
B
MPZ
MBP
PLP1
MAG
PRX
NCMAP
FABP7
KCNJ10/Kir4.1
CDH19
Classifications
Blood
Connective tissue
Endothelial
Macrophages
Mesenchymal
Neurons
Neutrophils
Pericytes
Satellite glial cells
Schwann
smooth muscle cells
T cells
N/A
C
SGC
Schwann
582
23
549
D
SGC
Astrocytes
512
93
407

Fig.2

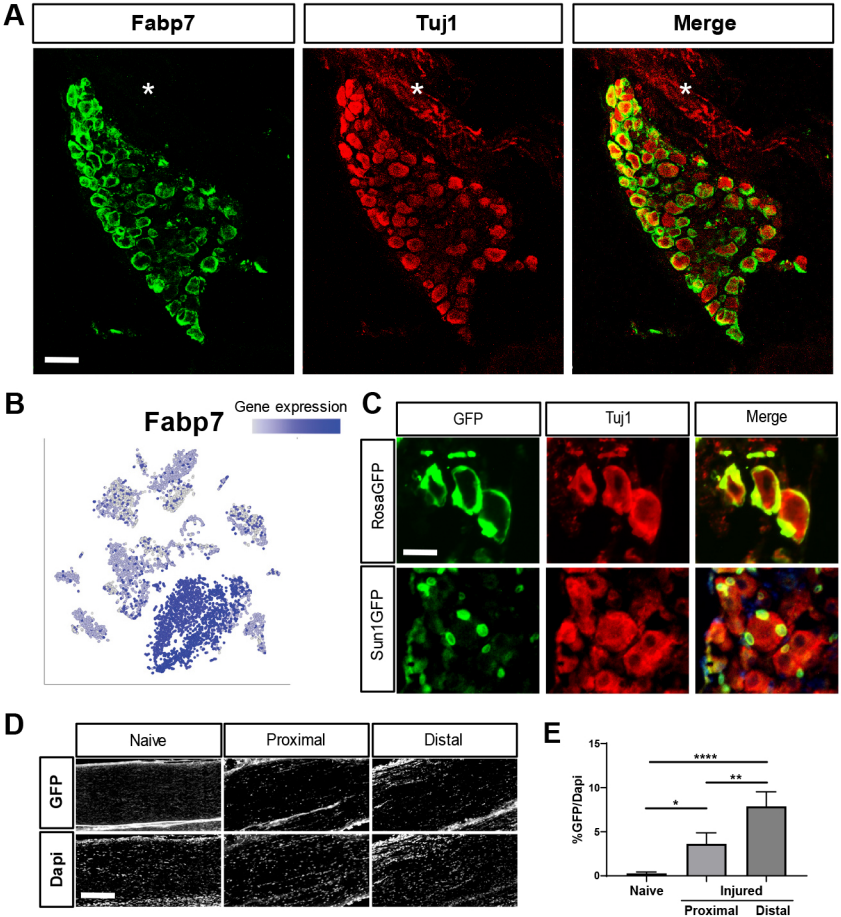
A
Fabp7
Tuj1
Merge
B
Fabp7
Gene expression
C
GFP
Tuj1
Merge
RosaGFP
Sun1GFP
D
Naive
Proximal
Distal
GFP
Dapi
E
%GFP/Dapi
15
10
5
0
****
**
*
Naive
Injured
Proximal
Distal

Fig.S2

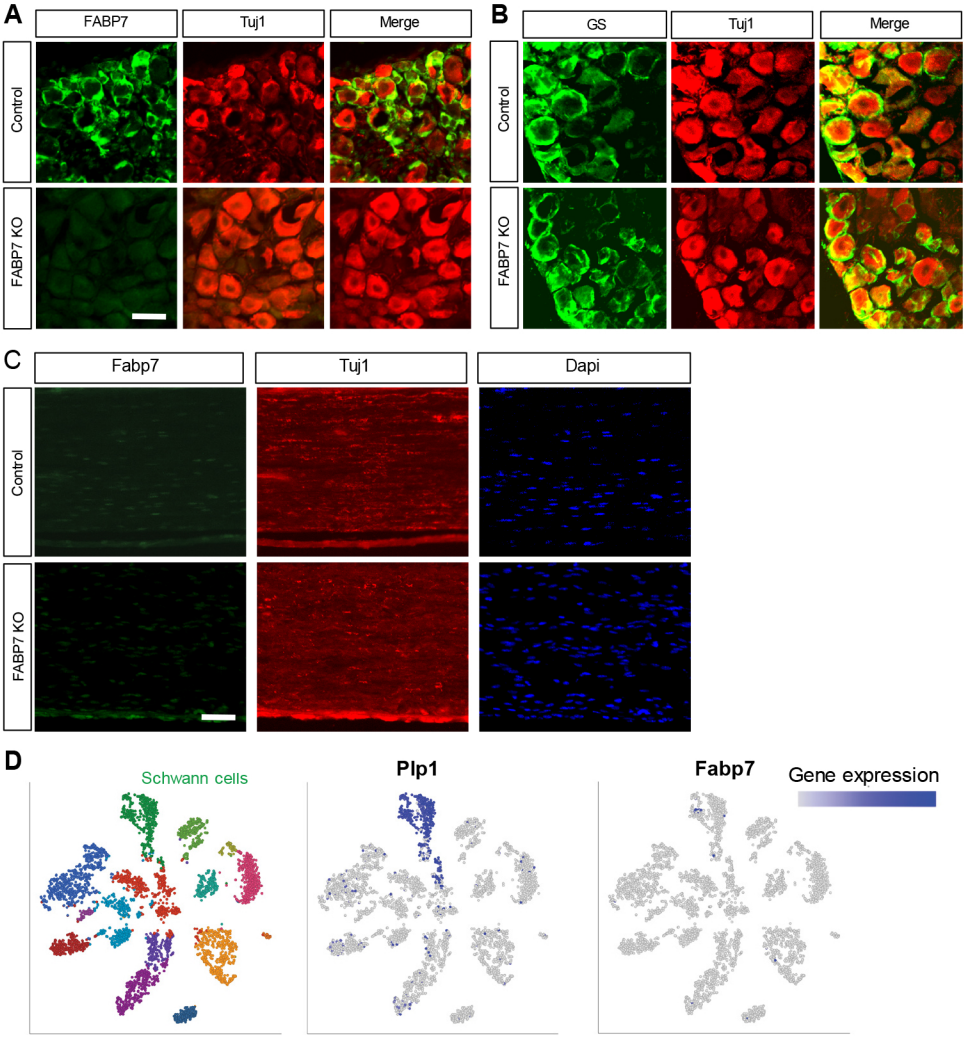
A
FABP7
Tuj1
Merge
Control
FABP7 KO
B
GS
Tuj1
Merge
Control
FABP7 KO
C
Fabp7
Tuj1
Dapi
Control
FABP7 KO
D
Schwann cells
Plp1
Fabp7
Gene expression

Fig.3

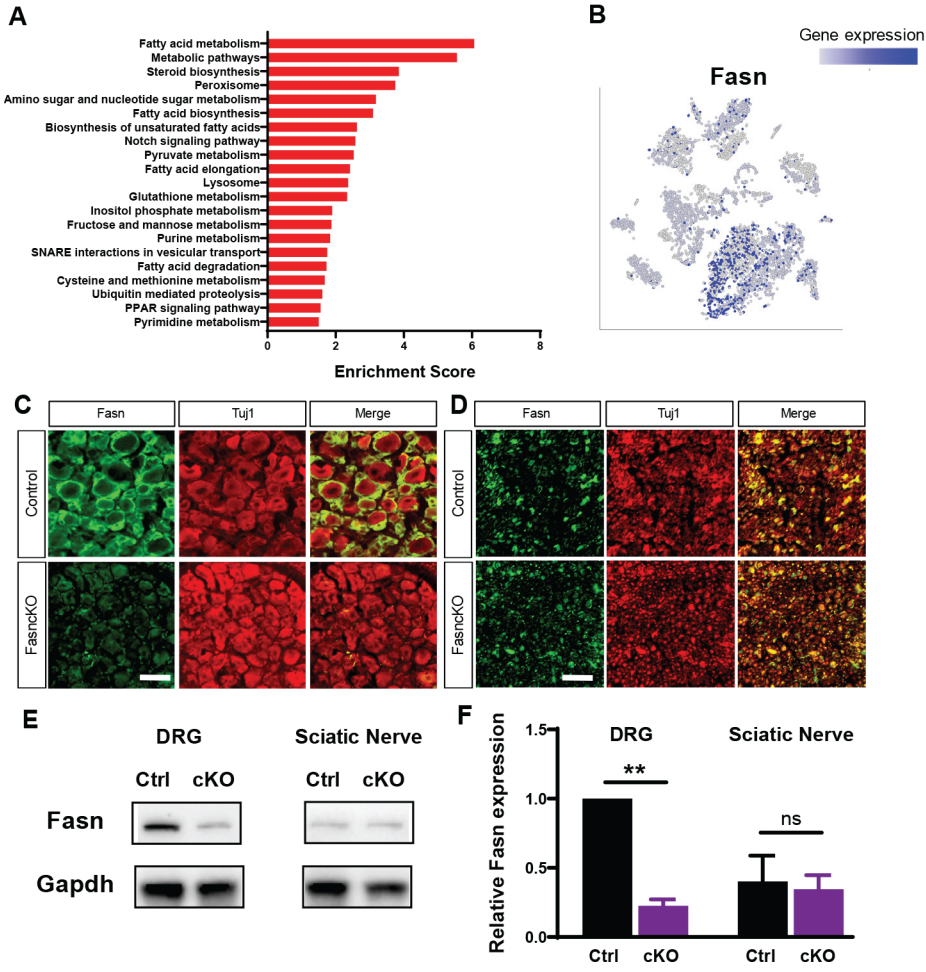
A
Fatty acid metabolism
Metabolic pathways
Steroid biosynthesis
Peroxisome
Amino sugar and nucleotide sugar metabolism
Fatty acid biosynthesis
Biosynthesis of unsaturated fatty acids
Notch signaling pathway
Pyruvate metabolism
Fatty acid elongation
Lysosome
Glutathione metabolism
Inositol phosphate metabolism
Fructose and mannose metabolism
Purine metabolism
SNARE interactions in vesicular transport
Fatty acid degradation
Cysteine and methionine metabolism
Ubiquitin mediated proteolysis
PPAR signaling pathway
Pyrimidine metabolism
0
2
4
6
8
Enrichment Score
B
Gene expression
Fasn
C
Fasn
Tuj1
Merge
Control
FasncKO
D
Fasn
Tuj1
Merge
Control
FasncKO
E
DRG
Sciatic Nerve
Ctrl
cKO
Ctrl
cKO
Fasn
Gapdh
F
DRG
Sciatic Nerve
Relative Fasn expression
1.5
1.0
0.5
0.0
**
ns
Ctrl
cKO
Ctrl
cKO

Fig.S3

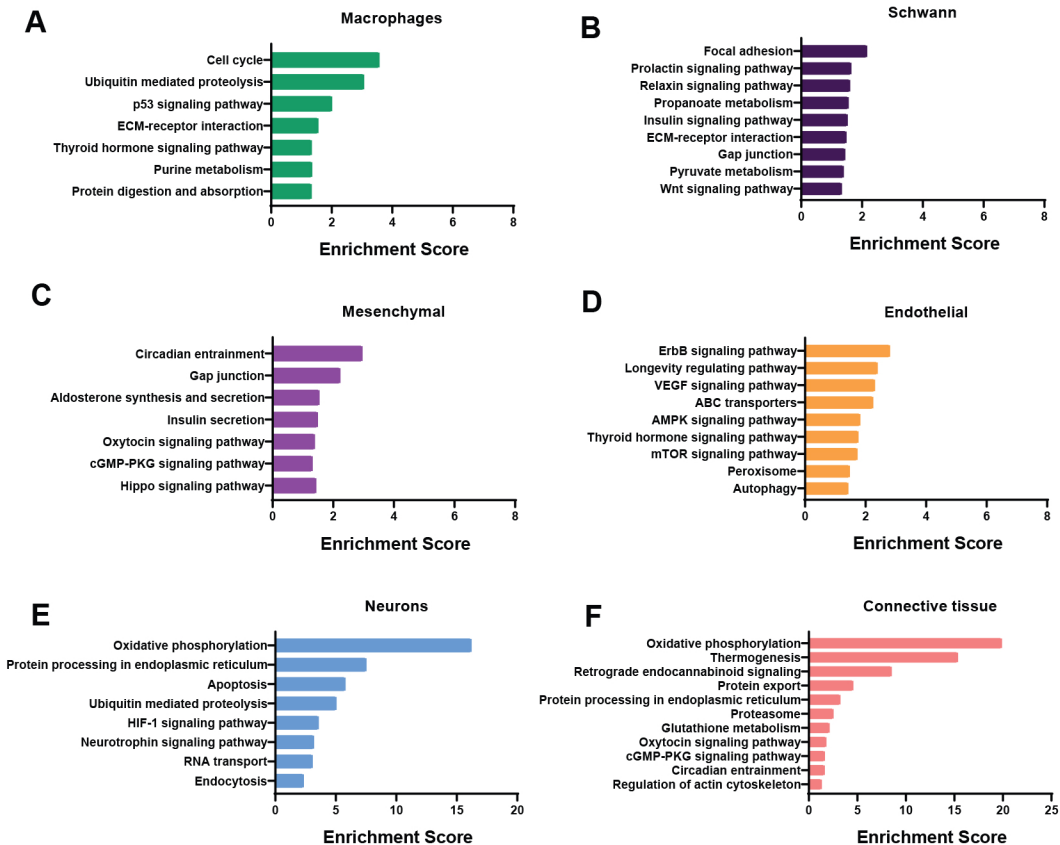
A
Macrophages
Cell cycle
Ubiquitin mediated proteolysis
p53 signaling pathway
ECM-receptor interaction
Thyroid hormone signaling pathway
Purine metabolism
Protein digestion and absorption
0 2 4 6 8
Enrichment Score
B
Schwann
Focal adhesion
Prolactin signaling pathway
Relaxin signaling pathway
Propanoate metabolism
Insulin signaling pathway
ECM-receptor interaction
Gap junction
Pyruvate metabolism
Wnt signaling pathway
0 2 4 6 8
Enrichment Score
C
Mesenchymal
Circadian entrainment
Gap junction
Aldosterone synthesis and secretion
Insulin secretion
Oxytocin signaling pathway
cGMP-PKG signaling pathway
Hippo signaling pathway
0 2 4 6 8
Enrichment Score
D
Endothelial
ErbB signaling pathway
Longevity regulating pathway
VEGF signaling pathway
ABC transporters
AMPK signaling pathway
Thyroid hormone signaling pathway
mTOR signaling pathway
Peroxisome
Autophagy
0 2 4 6 8
Enrichment Score
E
Neurons
Oxidative phosphorylation
Protein processing in endoplasmic reticulum
Apoptosis
Ubiquitin mediated proteolysis
HIF-1 signaling pathway
Neurotrophin signaling pathway
RNA transport
Endocytosis
0 5 10 15 20
Enrichment Score
F
Connective tissue
Oxidative phosphorylation
Thermogenesis
Retrograde endocannabinoid signaling
Protein export
Protein processing in endoplasmic reticulum
Proteasome
Glutathione metabolism
Oxytocin signaling pathway
cGMP-PKG signaling pathway
Circadian entrainment
Regulation of actin cytoskeleton
0 5 10 15 20 25
Enrichment Score

Fig.4

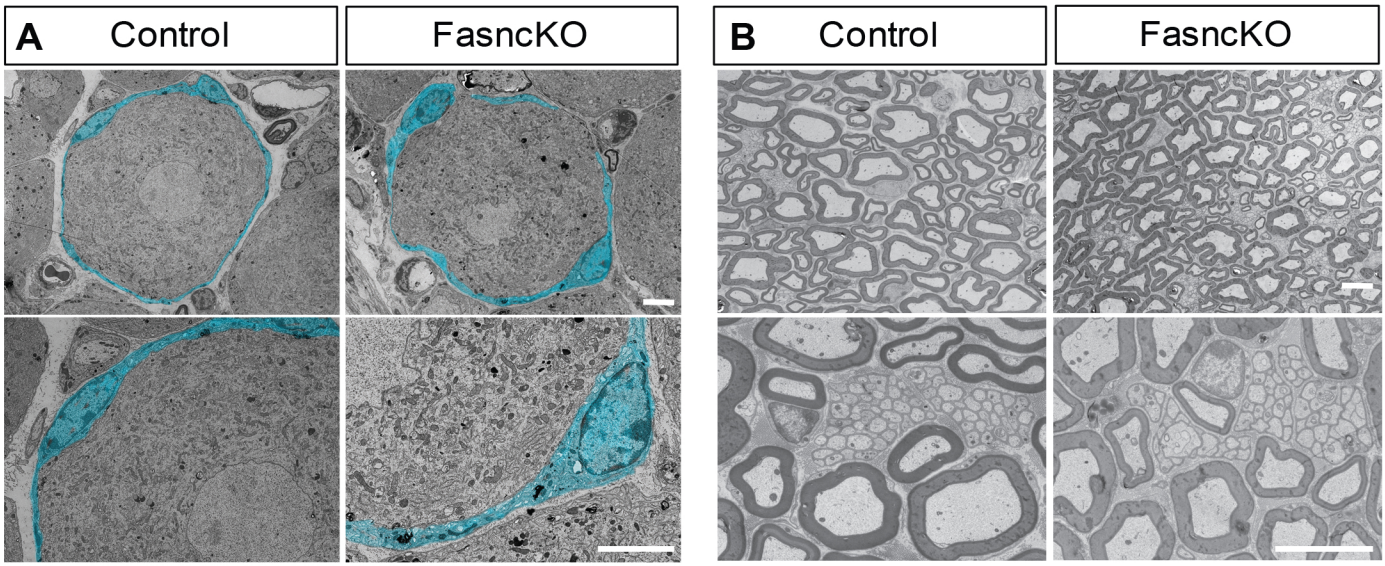
A
Control
FasncKO
B
Control
FasncKO

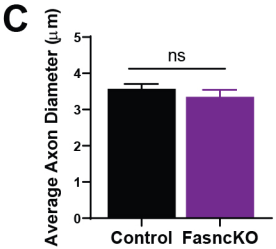
C
Average Axon Diameter (µm)
ns
Control
FasncKO

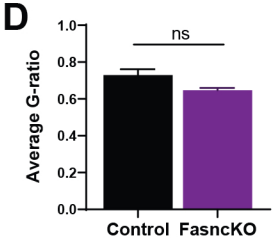
D
Average G-ratio
ns
Control
FasncKO

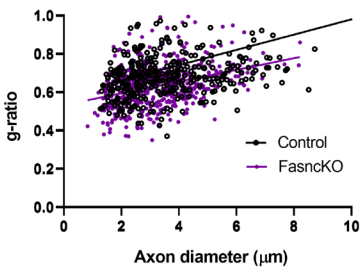
E
g-ratio
Control
FasncKO
Axon diameter (µm)

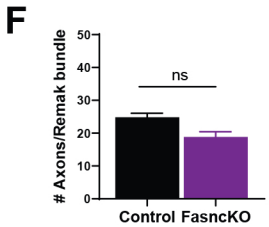
F
Axons/Remak bundle
ns
Control
FasncKO

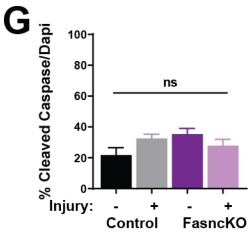
G
% Cleaved Caspase/Dapi
ns
Injury:
Control
FasncKO

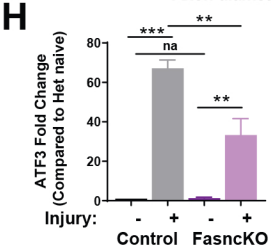
H
ATF3 Fold Change (Compared to Het naive)
***
na
**
**
Injury:
Control
FasncKO

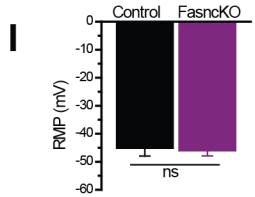
I
Control
FasncKO
RMP (mV)
ns

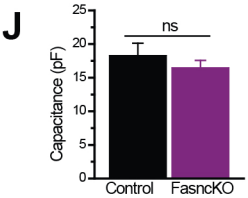
J
Capacitance (pF)
ns
Control
FasncKO

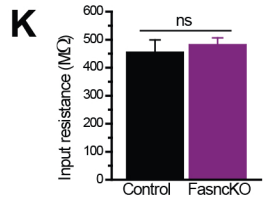
K
Input resistance (MΩ)
ns
Control
FasncKO

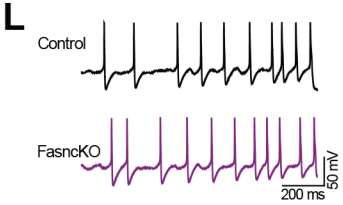
L
Control
FasncKO
200 ms
50 mV

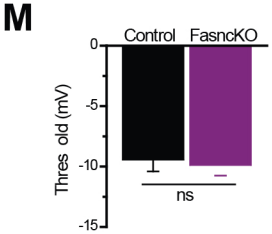
M
Control
FasncKO
Thres old (mV)
ns

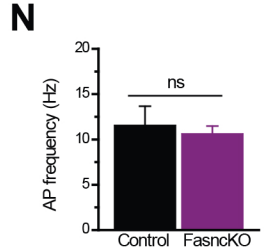
N
AP frequency (Hz)
ns
Control
FasncKO

Fig.S4

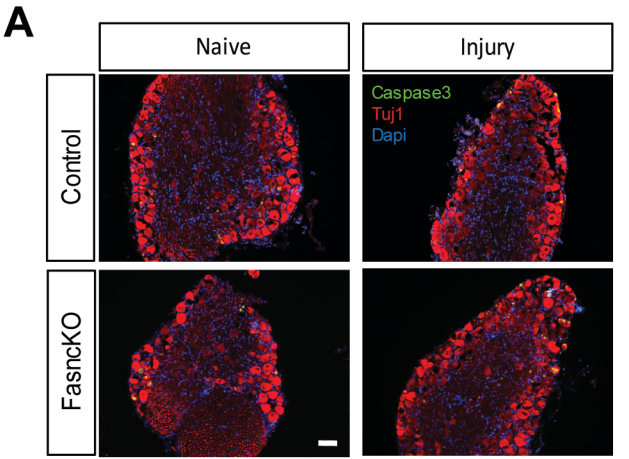
A
Naive
Injury
Control
FasncKO
Caspase3
Tuj1
Dapi

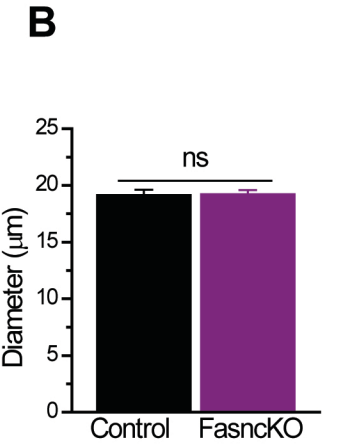
B
ns
Diameter (μm)
25
20
15
10
5
0
Control
FasncKO

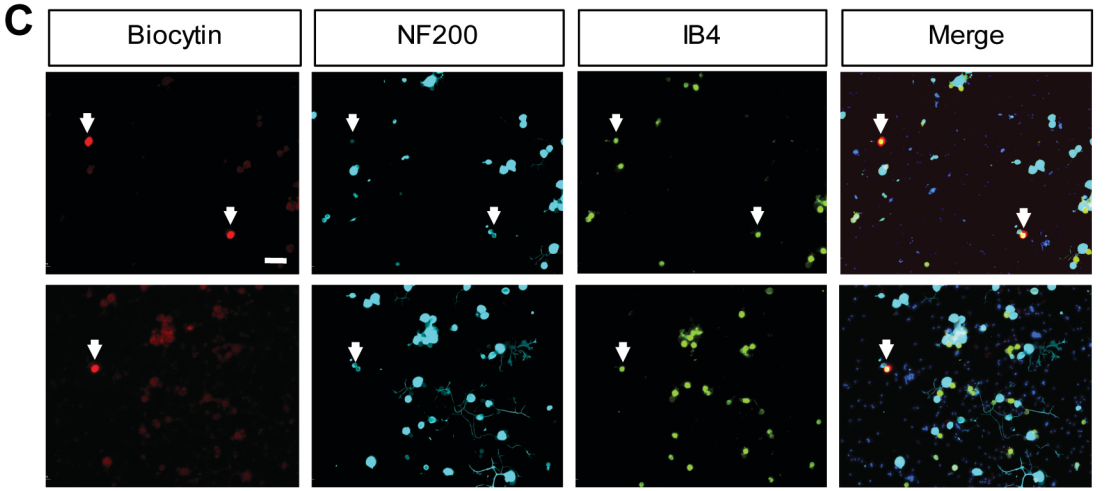
C
Biocytin
NF200
IB4
Merge

Fig.5

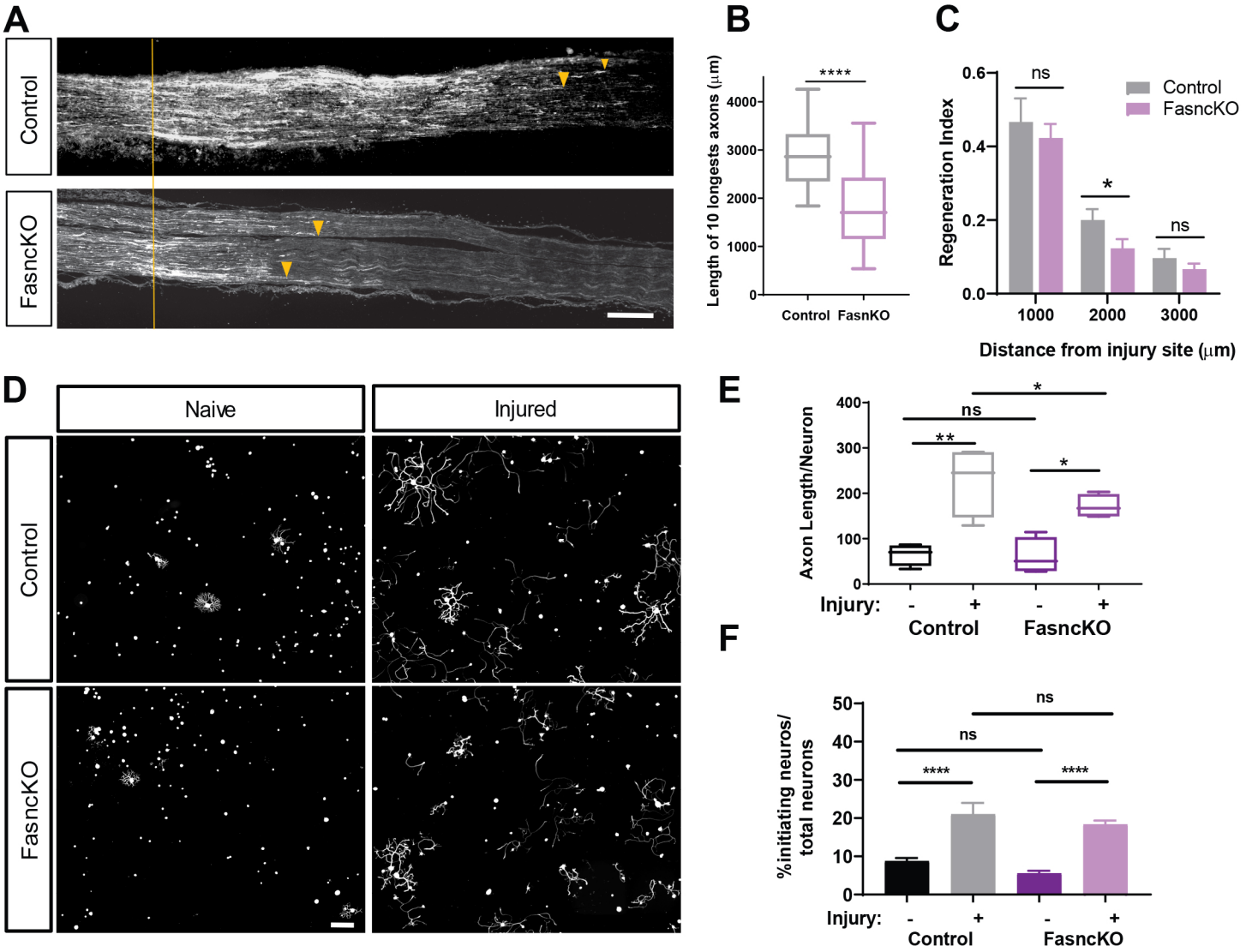
A
Control
FasncKO
B
Length of 10 longests axons (μm)
****
Control
FasnKO
C
Regeneration Index
ns
*
ns
Control
FasncKO
Distance from injury site (μm)
D
Naive
Injured
Control
FasncKO
E
Axon Length/Neuron
ns
**
*
*
Injury:
Control
FasncKO
F
%initiating neuros/ total neurons
ns
ns
****
****
Injury:
Control
FasncKO

Fig.6

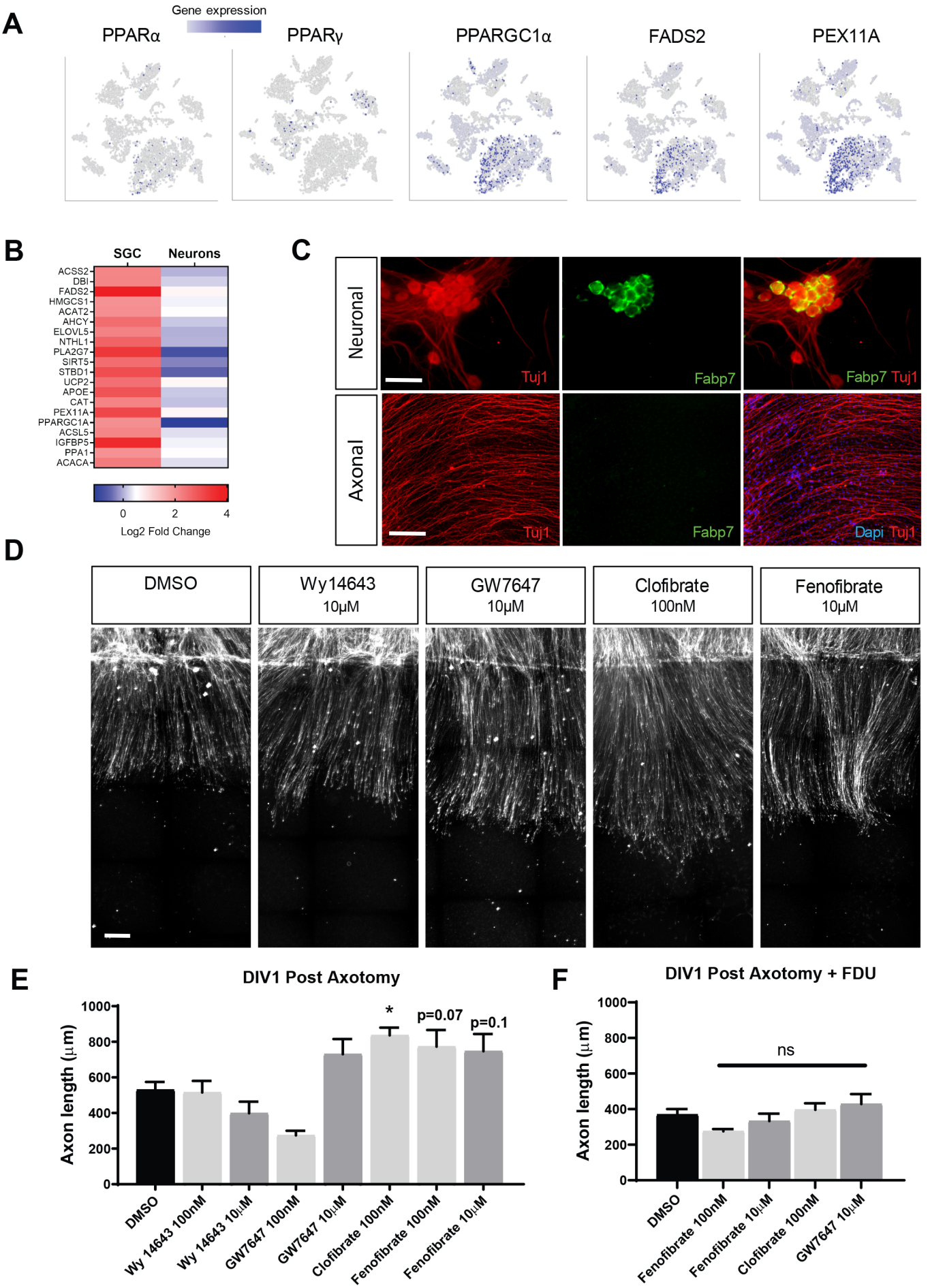
A
Gene expression
PPARα
PPARγ
PPARGC1α
FADS2
PEX11A
B
SGC
Neurons
ACSS2
DBI
FADS2
HMGCS1
ACAT2
AHCY
ELOVL5
NTHL1
PLA2G7
SIRT5
STBD1
UCP2
APOE
CAT
PEX11A
PPARGC1A
ACSL5
IGFBP5
PPA1
ACACA
0
2
4
Log2 Fold Change
C
Neuronal
Axonal
Tuj1
Fabp7
Fabp7 Tuj1
Dapi Tuj1
D
DMSO
Wy14643
10μM
GW7647
10μM
Clofibrate
100nM
Fenofibrate
10μM
E
DIV1 Post Axotomy
Axon length (μm)
1000
800
600
400
200
0
*
p=0.07
p=0.1
DMSO
Wy 14643 100nM
Wy 14643 10μM
GW7647 100nM
GW7647 10μM
Clofibrate 100nM
Fenofibrate 100nM
Fenofibrate 10μM
F
DIV1 Post Axotomy + FDU
Axon length (μm)
1000
800
600
400
200
0
ns
DMSO
Fenofibrate 100nM
Fenofibrate 10μM
Clofibrate 100nM
GW7647 10μM

Fig.S5

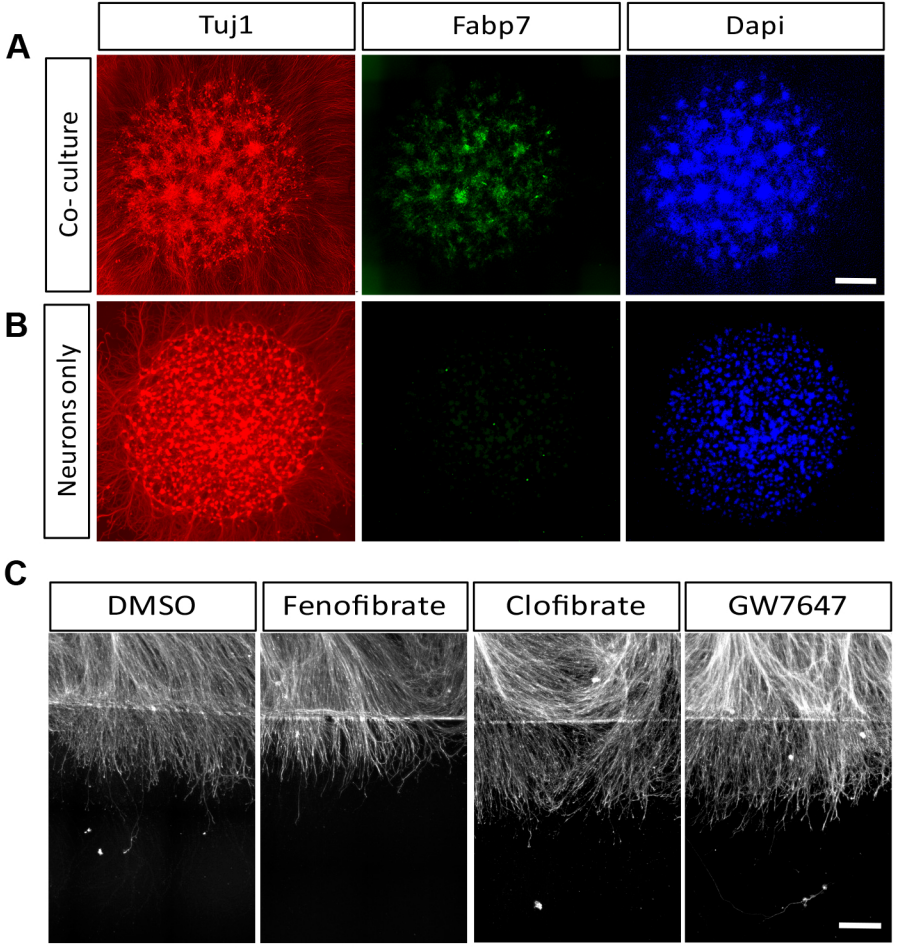
A
Tuj1
Fabp7
Dapi
Co- culture
B
Neurons only
C
DMSO
Fenofibrate
Clofibrate
GW7647

Fig.7

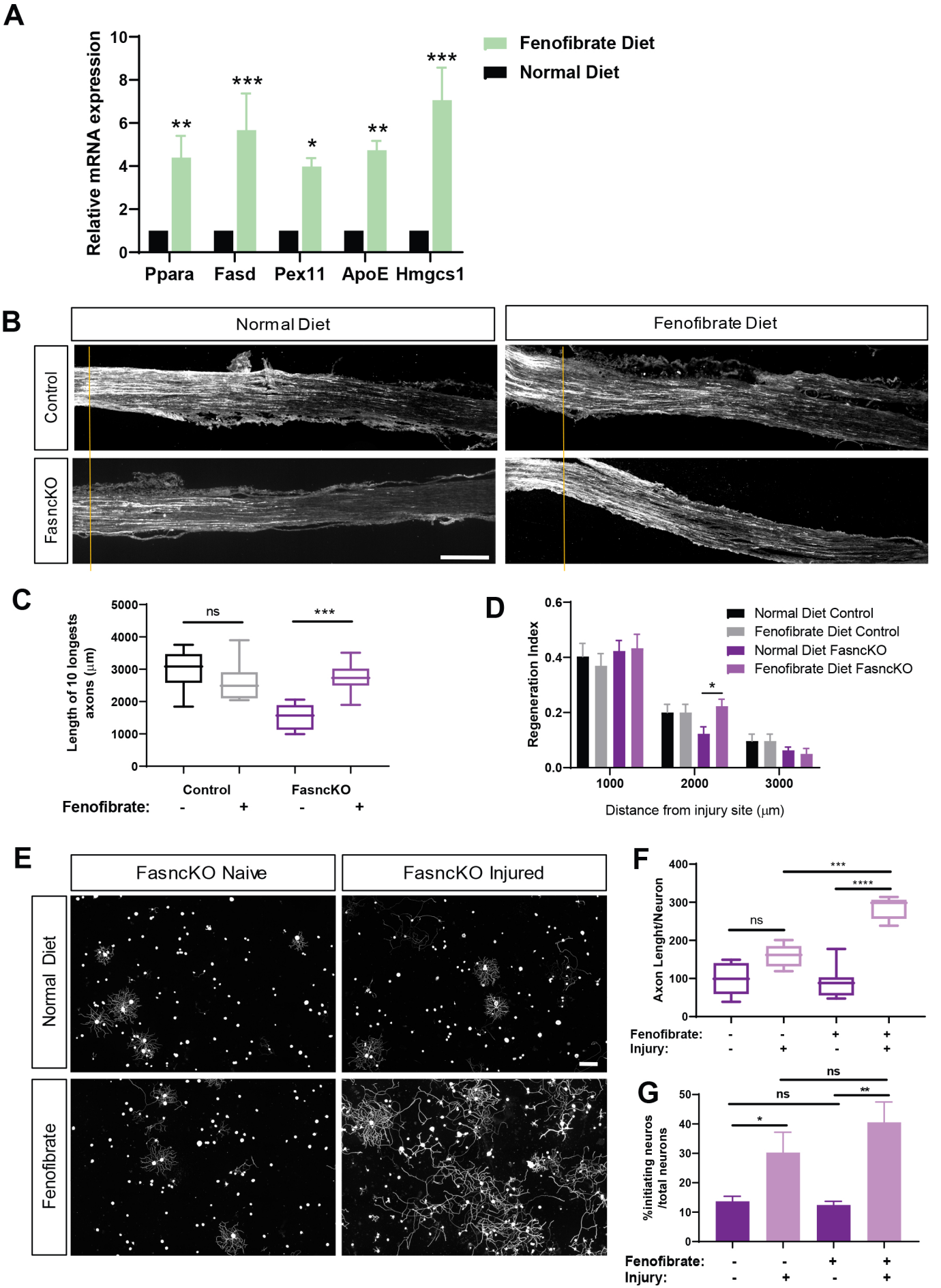
A
Relative mRNA expression
Fenofibrate Diet
Normal Diet
Ppara
Fasd
Pex11
ApoE
Hmgcs1
B
Normal Diet
Fenofibrate Diet
Control
FasncKO
C
Length of 10 longests axons (μm)
ns
***
Control
FasncKO
Fenofibrate:
D
Regeneration Index
Normal Diet Control
Fenofibrate Diet Control
Normal Diet FasncKO
Fenofibrate Diet FasncKO
Distance from injury site (μm)
E
FasncKO Naive
FasncKO Injured
Normal Diet
Fenofibrate
F
Axon Lenght/Neuron
Fenofibrate:
Injury:
G
%initiating neuros /total neurons
Fenofibrate:
Injury: